AD-A098 688 ROYAL AIRCRAFT ESTABLISHMENT FARNBOROUGH (ENGLAND) F/G 20/4
PRESSURE DISTRIBUTIONS ON SOME DELTA WINGS AT M=4.(U)
MAY 80 L C SQUIRE, K C MOORE
UNCLASSIFIED RAE-TR-80068 DRIC-BR-76040 NL

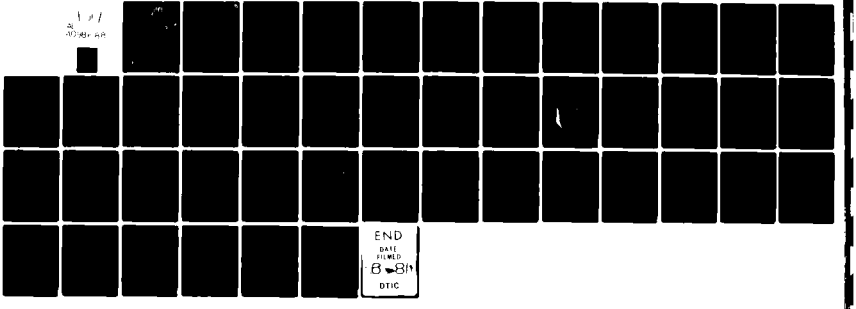

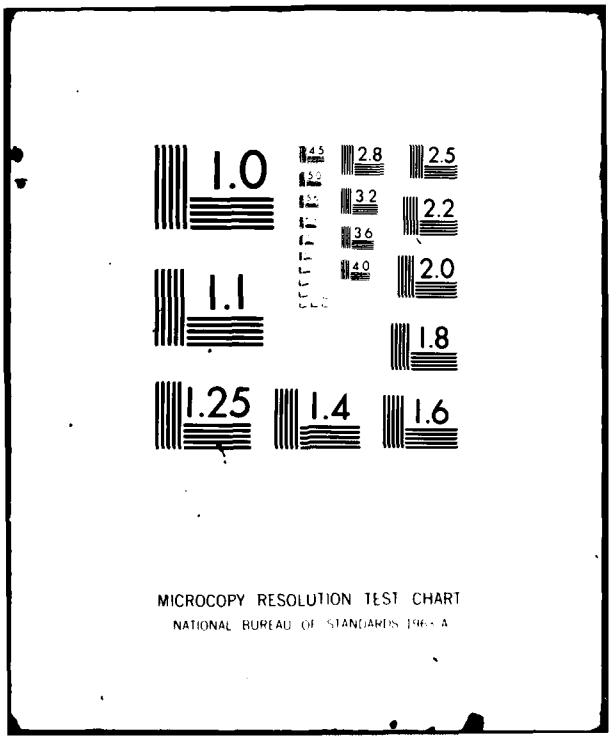
1.0
1.1
1.25
1.4
1.6
1.8
2.0
2.2
2.5
2.8
3.2
3.6
4.0
MICROCOPY RESOLUTION TEST CHART
NATIONAL BUREAU OF STANDARDS 1963-A

ROYAL AIRCRAFT ESTABLISHMENT

*

Technical Report 80068

May 1980

PRESSURE DISTRIBUTIONS ON SOME DELTA WINGS AT M=4.

by

46

L.C. Squire
K.C. Moore

RAE-TR-80068

*

DRIC BR-76040

Procurement Executive, Ministry of Defence
Farnborough, Hants

UDC 533.693.3 : 533.6.048.2 : 533.6.011.55

ROYAL AIRCRAFT ESTABLISHMENT

Technical Report 80068

Received for printing 22 May 1980

PRESSURE DISTRIBUTIONS ON SOME DELTA WINGS AT M = 4

by

L. C. Squire*

K. C. Moore**

SUMMARY

Complete pressure distributions are presented for a series of delta wings tested through an incidence range at a Mach number of 4. The results have been integrated to obtain lift and drag coefficients and the values found are in good agreement with the trend from measurements on similar wings at lower Mach numbers. Some of the models were designed to test a possible method of engine/airframe integration. The results show that it is possible to add volume to the rear of the wing without increasing the drag of the forebody, thus confirming the proposed method of integration.

Departmental Reference: Aero 3484

* Cambridge University Engineering Department, Consultant D/RAE.

** RARDE.

LIST OF CONTENTS

1 INTRODUCTION

This Report gives the results of pressure plotting tests made in the 3 ft x 4 ft tunnel at RAE Bedford on seven delta wings at a Mach number of 4. The first three models were planned in 1958 to study the effects of subsonic, sonic and supersonic leading edges at Mach numbers higher than normally associated with linearized supersonic wing theory. In fact the three models were geometrically similar to models then being tested in the 8 ft x 8 ft supersonic tunnel in connection with early studies for a supersonic transport. A full analysis of some of these 8 ft x 8 ft tunnel tests has recently been published by Weber and King[1]. The other four wings were designed to study the effects of integration of the power plant with usable volume[2]. The particular method of integration considered was based on the fact that the nozzle exit area of an air-breathing engine designed for Mach numbers above 4 is significantly greater than the inlet area, and it was thought that this increase in area could be combined with the usable volume to give a shape with a finite base area. It was further hoped that the zero-lift wave drag of the resultant shape apart from the base drag would be lower than that of the original wing volume with a sharp trailing edge. In an actual aircraft design it should then be possible to add a constant area duct, with an area equal to the engine intake area, to the blunt based wing shape. The engine could then be designed so that the nozzle filled the whole of the combined base area, but the overall drag should still be less than that of the usable volume alone. The full philosophy of this approach, together with a discussion of possible area distributions, is given in Ref 2, and the actual shapes chosen for testing are described in section 2.

The models were tested in 1962/3, but because of a change in design interests the preparation of the results was given a low priority. However, recently there has been renewed interest in the calculation of supersonic wave drag and in calculation methods for supersonic flow fields and it was felt that the pressure distributions obtained on the present series of wings might serve as a test case for these methods. In addition the results for the drag at zero lift form a useful supplement at higher Mach numbers to the results analysed by Weber and King.

2 DETAILS OF MODEL GEOMETRY

Six models were tested, one of them with and without a cylindrical body at the rear, making seven shapes in all. All the models had delta planforms and

diamond cross-sections normal to the length. Models* 1 to 3 all had 'Lord V' area distributions[3] with aspect ratios of 4/3, 1 and 2/3 respectively, and they were geometrically similar to models 234, 239 and 242[1] tested in the 8 ft x 8 ft tunnel. Model 4 was derived from model 3 by the addition of an area distribution varying like x^6, while model 5 was obtained from model 3 by the addition of an area distribution varying like x^2. In both cases the constant of proportionality was chosen so that the finite base area was equal to half of the maximum cross-sectional area of the combined shape. Model 6 was obtained by simply adding a circular cylindrical body to model 3 so that the base area was one half of the maximum cross-sectional area of model 3. Finally model 7 was designed to have the same longitudinal area distribution as model 6, but with the additional area spread across the section to give diamond cross-section throughout. Models 3 to 7 all had aspect ratio 2/3. Planform shapes are shown in Fig 1 and the longitudinal distributions of cross-sectional area in Fig 2. Details of the actual area distributions are given in the Appendix and further details of the model geometry in Table 1. Drawings of models 1 and 3, generated from their cross-sections seen in perspective, are shown in Fig 3.

All the models were fitted with pressure holes along the centreline and along chordwise lines at 0.2, 0.4, 0.6 and 0.8 of the semispan (see Fig 1). The actual hole positions are tabulated in Table 2. It will be noted that only a few holes were available along y/s = 0.2 for models 3 to 6.

In order to support the models in the tunnel it was necessary to add a small cylindrical body at the rear to shield the sting support system. This body was of 70 mm diameter for models 1 and 2 and of 84.3 mm diameter for the others. No shield was needed on model 6 since the sting could be contained within the basic shape. In addition the models could be mounted on an angled sting system which entered the model through one surface so that the other surface was undistorted. Methods for correcting for the shield effects are discussed in section 4.

3 DETAILS OF THE TESTS

The tests were made using the interim wooden nozzle of the 3 ft x 4 ft (0.914 m x 1.219 m) tunnel to give a Mach number of 3.96. The total pressure was 0.745 MN/m^2 and the total temperature was 40°C, giving a Reynolds number of $3.2 \times 10^7/m$. Humidity was held at less than 210 parts/million.

* The model numbers in the 3 ft x 4 ft tunnel were 301, 302, 303, 305, 307, 303b and 308 respectively.

Pressures were measured by Midwood self-balancing capsule manometers, and up to 15 min were allowed at each incidence to allow the pressures to settle; the results were then recorded on card. The normal accuracy of the system corresponds to ±0.001 in C_p, but at pressures less than 3 kN/m^2 (C_p = -0.03) there may be additional errors due to outgassing in the pressure tubes. These latter will give a positive bias to C_p.

Models 1 and 2 were tested over the incidence range -4^o to $+24^o$ with the model upright and inverted. Model 3 entered a violent pitching oscillation at 23^o so tests on the other models were restricted to 22^o. The angled sting configuration was tested over a pitch range from -4^o to $+24^o$, corresponding to an incidence range between $\pm 14^o$.

4 STING INTERFERENCE EFFECTS

The main series of tests were made using the straight sting system since this system produced the most accurate incidence settings. Two additional tests were conducted which would permit a correction to be made for sting interference effects. In these tests the model was mounted on an angled sting which entered it from one side, the opposite surface being either the true surface or one which featured a dummy sting shield. By suitable interpolation it should have been possible to deduce from these tests the sting interference effects at the incidences actually achieved in the main tests. A computer program was written to process the three sets of results from each model, and to plot the final corrected pressures. Some reservations were felt at the time about the results of this process, since certain small effects could not be easily explained, but the matter was not pursued since other work was given higher priority. By now, all that remains on file is the computer generated plots; the raw data and the computer program having apparently been destroyed. However, for reasons given in the introduction, it was thought worthwhile to rescue the results from obscurity. Since the only doubts about the validity of the data concern the sting interference effects, some simple tests to establish the likely magnitude of these effects were made in the supersonic tunnel at Cambridge University Engineering Department. In planning these tests it was noted that the centreline profiles of the models were almost straight in the region of the sting shield (see Fig 4) and that the portion of the cylindrical body which protruded from the model surface was similar to that obtained when a cylinder is cut by an oblique plane. It was decided to mount this shape on the side wall of the tunnel and to measure the resultant pressure field. The shape was cut from a circular cylinder of 25.4 mm diameter with the angle of the cut corresponding to the slope of the

centreline surface of models 1 to 3 (approximately 4.5^{o}). This shape was mounted on the centreline of the tunnel wall and pressures were measured along streamwise lines 25.4 mm, 50.8 mm and 76.2 mm above and below the centreline. These tests were made at Mach numbers of 2.5 and 3.5 at Reynolds numbers, based on length, of 5.5×10^{6} and 8.8×10^{6} respectively. In these tests the thickness of the wall boundary layer was about 7 mm. Results in the form $\Delta p/p_L$, where Δp is the pressure increment due to the body and P_L is the pressure in the absence of the body, are plotted in Fig 5. These results show that the magnitude of the interference pressure field falls away from the body and that the effects are confined to a triangular region which has its apex about 1.5 body diameters ahead of the nose of the model and is swept at the free-stream Mach angle. The actual magnitude of $\Delta p/p_L$ is slightly greater at M = 3.5 than at M = 2.5. It is possible to convert the measured pressure differences to pressure coefficients at M = 3.96 by noting that the pressure over the rear of the wings is approximately constant and so we may assume that the body is in a uniform flow field for which the local pressure P_L is given by:

$$P_L = p_\infty \left(1 + \frac{\gamma M_\infty^2}{2} C_p\right) ,$$

where M_∞ is the stream Mach number (3.96), and p_∞ is the stream static pressure. Thus ΔC_p is given by

$$\Delta C_p \equiv \frac{\Delta p}{p_\infty} \frac{2}{\gamma M_\infty^2}$$

$$= \frac{\Delta p}{p_L} \frac{2}{\gamma M_\infty^2} \left(1 + \frac{\gamma M_\infty^2}{2} C_p\right)$$

$$= \frac{\Delta p}{p_L} \left(\frac{2}{\gamma M_\infty^2} + C_p\right)$$

$$= \frac{\Delta p}{p_L} \left(0.091 + C_p\right) \quad .$$

This formula has been used to estimate the magnitude of the sting effect on the actual model, by assuming that at each value of y/d the maximum value of $\Delta p/p_L$ varies linearly with the local Mach number. It has been further assumed that this Mach number can be found from C_p by the isentropic relations. The resultant maximum values of ΔC_p at y/d = 1 and 2 are plotted in Fig 6 against the local value of C_p.

The interference results from Figs 5 and 6 were mainly used to establish the actual regions of interference on the models and to find the possible magnitude of the corrections which might have been applied in these regions. In one case, however, they have been used to correct what appears to be a genuine error in the plotted results. This error occurs in the centre at the rear of model 3 where the plotted pressures are higher than at corresponding points on model 6. As will be recalled, model 6 was obtained from model 3 by the addition of a circular body at the rear so that no correction was needed for sting-shield interference. The results for model 6 were consistent with those for models 4 and 5 so the results for model 3 were clearly in error. This error hampered the analysis of the results, particularly at zero-lift, and it was decided to subtract the interference pressures, as found in the Cambridge tests, from the results for model 6 to get 'corrected' zero-lift results for model 3. These 'corrected' results are plotted in Figs 11, 12, 14 and 15 and are used in the drag calculations. However, the pressures for model 3 plotted in Figs 9 and 10 are not corrected in this way.

5 PRESENTATION AND DISCUSSION OF RESULTS

5.1 Presentation of basic results

The basic results for models 1 and 2 are plotted in Figs 7 and 8 for incidences of 0, 4, 8, 12, 16, 20 and 24° on both surfaces. The results downstream of the sloping lines shown for $y/s = 0.2$, 0.4 and 0.6 are in the region of possible interference from the sting shield and may be subject to error. An interesting feature of these results is the increase in pressure which occurs towards the trailing edge for $y/s \leq 0.4$. At first sight it might be thought that this increase in pressure is due to shield interference, but this is unlikely since it is also present on the centreline (Figs 7a and 8a) where the pressures must have been measured on the clean surface of the model using the angled sting system since pressure holes were not placed on the sting shields. The effect is also present at low incidence along $y/s = 0.4$ at points well ahead of the region of interference.

Corresponding results for models 3 to 5 and for models 3, 6 and 7 are plotted in Figs 9 and 10 respectively. In these figures the measured results for model 3 are plotted as symbols and the results for the other models are represented by lines drawn through the measured points *where these measured points differ from the results for model 3*. For example, on the centreline of models 3 to 5 (Fig 9a) the results on the suction surfaces for the three wings

are identical to plotting accuracy so that only results for model 3 are shown. In the same figure the results for model 5 only differ from those for model 3 over the last 20% of the chord, elsewhere they are identical to those for model 3*. As for models 1 and 2 the results for model 3 show an increase in pressure towards the trailing edge for $y/s \leq 0.4$, but here the actual behaviour is less clear since, as noted above, the pressures measured on model 3 are higher than measured on model 6 with the body (Fig 10b), and are almost certainly in error in this region.

These results are now considered in more detail starting with the pressure at zero incidence.

5.2 Results at zero incidence

Pressure distributions on the three basic wings (models 1 to 3) at zero incidence are compared in Figs 11 and 12. Fig 11 compares the pressures along chordwise lines whereas Fig 12 shows contour plots. Two sets of results for model 3 are shown in Fig 11. The straight crosses show the original results whereas the solid points were obtained by subtracting the shield interference pressures from the results for model 6 as explained in section 4. It is thought that these corrected results are the more reliable and the contours of Fig 12 are based on them, as are the drag coefficients calculated below. From Figs 11 and 12 it is clear that in all cases the pressure is highest at the leading edge but that it falls rapidly inboard reaching a minimum in a region parallel to the leading edge (Fig 12). In all cases the pressure rises again in a triangular region near the centre of the trailing edge. For the reasons discussed in the last section this rise in pressure is thought to be genuine and not due to shield interference.

Results for the three models have been integrated to give drag coefficients. This integration has been carried out in two ways. Originally K.C. Moore developed a series of weighting functions for each pressure hole so that the drag coefficient was given by $\sum_1 w_i C_{p_i}$. The values obtained were checked by plotting C_p against z for each spanwise station and integrating the area under the curve to obtain sectional drag coefficients, and these were then integrated

* As a caveat to this statement it should be pointed out that the pressures measured on the first three holes along the centreline tended to show an erratic behaviour on all the models. These holes are on a very sharp ridge and are strongly influenced by slight misalignment of the models. The results plotted for model 3 are in fact the mean of the measured values for models 3, 4, 6 and 7, since these models are identical at the nose.

across the span. The results from the two methods are shown in Table 3 and it will be seen for each wing the two estimates agree to within 0.0002 in C_D. These coefficients are believed to be free from any error arising out of interference effects from the sting shield, however, Table 3 includes an additional column of ΔC_D. This value was obtained by assuming a constant increment of 0.008 in C_p (see Fig 6) acting over the whole region of interference from the support. This value of ΔC_D is only included as an indication of the worst error which could arise from this source, rather than as a correction to be applied.

As mentioned in the introduction models 1 to 3 are identical to three models tested in the 8 ft x 8 ft tunnel at RAE Bedford at Mach numbers up to 2.8. The results of these tests have recently been analysed by Weber and King[1] who plotted the zero lift drag in terms of K_0, the ratio of the wave drag of the given wing to that of the Sears-Haack body of the same length and volume, *ie*

$$K_0 = \frac{\pi}{128} \frac{D_w}{\frac{1}{2}\rho V^2 c_0^2} \frac{1}{(Vol/c_0^3)^2} ,$$

where D_w is the wave drag, c_0 is the root chord and Vol the wing volume. The values of K_0 from the present tests at M = 4 are in good agreement with the values found by Weber and King[1] at lower Mach number (Fig 13).

Pressure distributions at zero incidence for models 3 to 5 are plotted in Fig 14 and corresponding results for models 3, 6 and 7 in Fig 15. In these figures all the pressures for model 3 are plotted by round symbols and the results for the other models only plotted where they differ from those for model 3. Fig 14 also includes theoretical pressure distributions for the three wings obtained from linearized supersonic thin-wing theory. As will be seen the measured pressures are higher than the linear theory values although the shapes are similar, except that the increase in pressure at the centre rear of model 3 is not predicted by theory*. The results in Fig 15 also show that over the whole of the wing surface the pressures on models 6 and 7 are almost identical. If genuine, this shows that the pressure distribution in this particular case is controlled by the longitudinal distribution of area rather than by cross-sectional shape.

---

* This pressure rise is less evident in the 'corrected' results.

Drag coefficients for the bluff-based models (4, 5 and 7) are tabulated in Table 3. In these cases it was assumed that the bluff base was acted on by free stream static pressure, so that base drag was neglected. This is a reasonable way to compare different shapes if we are entitled to assume that the whole of the base area is available for exploitation when we come to integrate the propulsion system. The drag acting forward of the base was again calculated by both the methods discussed previously. This time the results of the two methods vary by up to 0.0004, with the largest discrepancy on model 7. For this model the original value is much lower than the recalculated value. Since the drag loops for model 7 are similar to those for model 4, and close to those for model 3 (see Fig 16) it would appear that the recalculated drag is the more accurate. The measured drag coefficient of model 3 is about 65% of the linear theory value (Table 3) and this reduction is in line with the conclusions of Weber and King. For the models with bluff bases the measured drag is closer to the theoretical values but models 4 and 7 still have lower drags than model 3 in spite of the large increase in volume. The drag of model 5 is greater than that of model 3 (C_D = 0.0020 compared with 0.0017), but in this case there is a 30% increase in volume. Since drag is proportional to the square of volume (for given plan area and thickness distribution) the drag of model 5 is also much less than that of a wing of equal volume with a sharp trailing edge. The ratio drag/(volume)^2 is in fact 0.70 for model 4, 0.66 for model 5 and 0.63 for model 7, if model 3 is taken to give a reference value of 1.00. Thus the results for the models with bluff trailing edges show that it is possible to add volume at the rear with a reduction in drag, although the actual reduction is less than that predicted by linear theory.

5.3 Pressure distributions at incidence

The pressure distributions for models 1, 2, 3, 4, 5 and 7 for incidences up to 12° were integrated by Moore to obtain C_L and C_D using his weighting functions. Results for C_L and C_D are plotted in Figs 17 and 18. Fig 17 also includes the linear theory values for the basic wings, and it will be noted that the measured lift is always below the linear theory value. It is also interesting to note that on all the models, except model 1, the variation of lift with incidence is non-linear. For the wings of aspect ratio 2/3 the thickest wing (wing 7) appears to produce the most lift.

The drag coefficients are plotted against C_L^2 in Fig 18 and in all cases the points lie on straight lines. Values of the lift-dependent drag factor

obtained from these lines are tabulated in Table 3 and the results for the basic wings are compared with results at lower Mach numbers in Fig 19. The present results are all just above the linear theory values with no leading-edge suction and are in excellent agreement with the trend of the results obtained at lower speeds.

Fig 20 compares the pressure distributions across the span at various chordwise stations on model 1 with measured distributions on two conical models of the same aspect ratio. Near the nose of the model the measured pressure distributions are similar to those found on the thick conical model, but aft of X = 0.25 the pressures are similar to those on the flat (*ie* thin) wing. Unfortunately measured results are not available for conical wings of aspect ratio 1 and 2/3.

Finally Fig 21 compares the results for model 1 at 24^{o} incidence with two theoretical estimates based on (a) thin-shock-layer theory combined with shock expansion theory[4] and (b) non-conical thin-shock-layer theory[5]. A full discussion of these theories and of their application to the present results will be found in Refs 4 and 5.

6 CONCLUDING REMARKS

The analysis of the results presented in this note has been hampered by the long delay since the tests were completed and by the failure to trace the original raw data. In particular there must be doubts about the accuracy of the measured pressures in the region influenced by the sting shield, although some of these doubts have been removed by the additional tests made at Cambridge. In fact the good agreement of the zero-lift drag coefficients with results on similar wings at lower Mach numbers would suggest that the results have been reasonably well corrected for interference effects.

The measured drags of the models with blunt bases confirm that it is possible to add volume to a basic wing with a sharp trailing edge so as to reduce the forebody drag. However, the actual reductions are less spectacular than originally thought possible. In part this may be because the drag of the basic shape is lower than estimated and therefore the scope for drag saving is less.

Also, of course, the estimated reductions were based on linear theory, which is unlikely to be reliable at M = 4. Indeed, one of the reasons for the delay in publishing the present results, was the change in interest which came

from the realisation that integrated shapes could be designed using non-linear theories, by means of the 'waverider' concept[6-9]. As design techniques, both methods have limitations. Linear theory permits us to consider a wider variety of shapes, but only to evaluate them approximately. The waverider approach allows the accurate evaluation of a limited class of shapes. A fair comparison between the two methods would be a very elaborate exercise, and far beyond the scope of the present paper.

Little analysis has been carried out on the pressure distributions at incidence, but it is considered that these pressure distributions will provide useful test cases for numerical methods in supersonic flow, as demonstrated by the results plotted in Fig 21.

Appendix

DETAILS OF LONGITUDINAL DISTRIBUTIONS OF CROSS-SECTIONAL AREA

Models 1 to 3 have 'Lord V' distributions of cross-sectional area given by

$$s(X) = 0.28(V/c_0)X^2(1 - X)(1 - 3X/2 + X^2 - X^3/4)$$

where $s(X)$ is the cross-sectional area at X $(= x/c_0)$ and x is the streamline distance from the vertex. V is the volume and c_0 the root chord.

Models 4 and 5 have this area distribution modified by the addition of a sextic and quadratic term respectively, *ie*

$$s(X)_4 = s(X)_3 + 7179\ X^6$$

$$s(X)_5 = s(X)_3 + 8710\ X^2 \quad .$$

In these distributions the constant is measured in square millimetres and was chosen so that the base area is half of the maximum cross-section area of the wing.

Models 1 to 5 all have diamond cross-sections.

Model 6 was obtained from Model 3 by the addition of a cylindrical body of diameter 95.59 mm at the rear of the wing. Again this body was chosen so that the base area is half of the maximum cross-sectional area of model 3. Model 7 has the same area distribution as model 6, but the additional area added is spread across the wing so that this model has diamond cross sections. This area distribution cannot be expressed easily in algebraic terms, but the addition to the root profile for model 7 is tabulated below.

Additional root profile model 7, (no change for $X < 0.583$)

X	Δh
0.6	0.88 mm
0.65	2.58 mm
0.7	4.36 mm
0.75	6.16 mm
0.8	7.92 mm
0.85	9.62 mm
0.9	11.21 mm
0.95	12.72 mm
1.0	14.12 mm

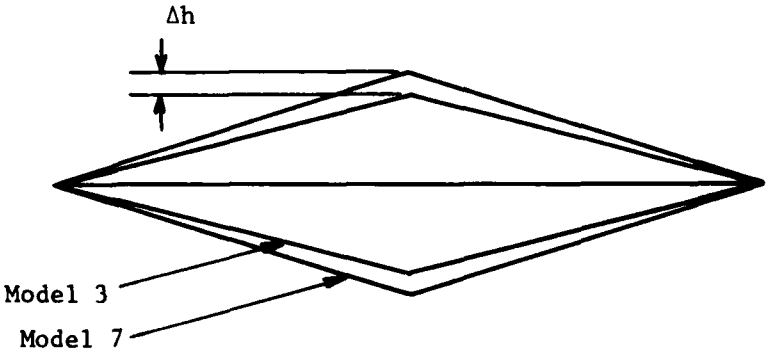

Table 1

DETAILS OF MODELS

Model number	1	2	3	4	5	7
Aspect ratio	4/3	1	2/3	2/3	2/3	2/3
Leading edge sweep angle	71.6^{o}	76^{o}	80.5^{o}	80.5^{o}	80.5^{o}	80.5^{o}
Semi-span (s)	0.323 m	0.298 m	0.254 m	0.254 m	0.254 m	0.254 m
Root chord (c_0)	0.969 m	1.192 m	1.524 m	1.524 m	1.524 m	1.524 m
Volume/c_0^3	0.0075	0.00562	0.00375	0.00419	0.00500	0.00444
Volume parameter (τ)	0.039	0.045	0.055	0.062	0.073	0.065
Base area (mm^2)	0	0	0	7179	8710	7176
$\beta s/c_0$ (at M = 4)	1.291	0.968	0.645	0.645	0.645	0.645

Table 2

COORDINATES OF PRESSURE HOLES

Hole No.	y/s	$\frac{x - x_{Leading\ edge}}{(local\ chord\ length)}$				
		Model 1&2	Model 3(&6)	Model 4	Model 5	Model 7
1	0	0.01	0.01	0.01	0.01	0.01
2	0	0.025	0.025	0.025	0.025	0.025
3	0	0.05	0.05	0.05	0.05	0.05
4	0	0.10	0.10	0.10	0.10	0.10
5	0	0.15	0.15	0.15	0.15	0.15
6	0	0.20	0.20	0.20	0.20	0.20
7	0	0.30	0.30	0.30	0.30	0.30
8	0	0.40	0.40	0.40	0.40	0.40
9	0	0.50	0.50	0.50	0.50	0.50
10	0	0.60	0.60	0.60	0.60	0.60
11	0	0.70	0.70	0.70	0.70	0.70
12	0	0.80	0.80	0.80	0.80	0.80
13	0	0.85	0.85	0.85	0.85	0.90
14	0	0.90	0.90	0.90	0.90	0.95
15	0	0.95	0.95	0.95	0.95	0.975
16	0	0.975	0.975	0.975	0.975	-
17	0	0.99	0.99	0.99	0.99	-
18	0.2	0.025	0.025	0.025	0.025	0.025
19	0.2	0.05	0.05	0.05	0.05	0.05
20	0.2	0.10	0.10	0.10	0.10	0.10
21	0.2	0.15	0.15	0.15	0.15	0.15
22	0.2	0.20	0.20	0.20	0.20	0.20
23	0.2	0.30	0.30	0.30	0.30	0.30
24	0.2	0.40	-	-	-	0.40
25	0.2	0.50	-	-	-	0.50
26	0.2	0.60	-	-	-	0.60
27	0.2	0.70	-	-	-	0.70
28	0.2	0.80	-	-	-	0.80
29	0.2	0.85	-	-	-	0.90
30	0.2	0.90	-	-	-	0.95
31	0.2	0.95	-	-	-	0.975
32	0.2	0.975	-	-	-	-
33	-	-	-	-	-	-
34	0.4	0.025	0.025	0.025	0.025	0.025
35	0.4	0.05	0.05	0.05	0.05	0.05
36	0.4	0.10	0.10	0.10	0.10	0.10
37	0.4	0.15	0.15	0.15	0.15	0.15
38	0.4	0.20	0.20	0.20	0.20	0.20
39	0.4	0.30	0.30	0.30	0.30	0.30
40	0.4	0.40	0.40	0.40	0.40	0.50
41	0.4	0.50	0.50	0.50	0.50	0.60
42	0.4	0.60	0.60	0.60	0.60	0.70
43	0.4	0.70	0.70	0.70	0.70	0.80
44	0.4	0.80	0.80	0.80	0.80	0.85
45	0.4	0.85	0.85	0.85	0.85	0.90
46	0.4	0.90	0.90	0.90	0.90	0.95
47	0.4	0.95	0.95	0.95	0.95	0.975
48	0.4	0.975	0.975	0.975	0.975	-
49	0.6	0.05	0.05	0.05	0.05	0.05
50	0.6	0.10	0.10	0.10	0.10	0.10
51	0.6	0.15	0.15	0.15	0.15	0.15
52	0.6	0.20	0.20	0.20	0.20	0.20
53	0.6	0.30	0.30	0.30	0.30	0.30
54	0.6	0.40	0.40	0.40	0.40	0.40
55	0.6	0.50	0.50	0.50	0.50	0.50
56	0.6	0.60	0.60	0.60	0.60	0.60
57	0.6	0.70	0.70	0.70	0.70	0.70
58	0.6	0.80	0.80	0.80	0.80	0.80
59	0.6	0.85	0.85	0.85	0.85	0.85
60	0.6	0.90	0.90	0.90	0.90	0.90
61	0.6	0.95	0.95	0.95	0.95	0.95
62	0.8	0.30	0.30	0.30	0.30	0.10
63	0.8	0.40	0.40	0.40	0.40	0.20
64	0.8	0.50	0.50	0.50	0.50	0.30
65	0.8	0.60	0.60	0.60	0.60	0.40
66	0.8	0.70	0.70	0.70	0.70	0.50
67	0.8	-	-	-	-	0.60
68	0.8	-	-	0.90	0.90	0.70
69	0.8	-	-	-	-	0.80
70	0.8	-	-	-	-	0.90
71	0.8	-	-	-	-	0.95

Table 3

DRAG COEFFICIENTS

(a) Drag coefficients at zero lift

Model	C_{D_0} (Theory)	C_{D_0} (KCM)	C_{D_0} (LCS)	ΔC_{D_0}
1		0.00318	0.0030	0.00026
2		0.00243	0.0023	0.00021
3	0.00251	0.00151*	0.0017	0.00028
4	0.00182	0.00133	0.0015	
5	0.00235	0.00216	0.0020	0.00017
7		0.00109	0.0015	

* This value is based on the 'original' pressures whereas the next (LCS) value is based on the 'corrected' pressures, see section 5.2

(b) Lift-dependent drag factor ($K = \pi A(C_D - C_{D_0})/C_L^2$)

Model	K
1	4.2
2	3.7
3	2.7
4	2.8
5	2.6
7	2.7

LIST OF SYMBOLS

A	aspect ratio
c_0	centreline chord
C_p	pressure coefficient
C_D	drag coefficient
C_L	lift coefficient
d	diameter of sting shield
D_W	wave drag
K_0	zero-lift wave drag factor
K	lift-dependent drag factor
M	Mach number
Δp	pressure increment due to sting shield
p_L	local pressure without sting shield
p	static pressure
s	semispan of wing
V	velocity of free stream
Vol	wing volume
w_i	weighting factor
x	streamwise coordinate
X	x/c_0
y	spanwise coordinate
z	coordinate normal to x, y
τ	'volume factor' = (volume) ÷ (wetted area)$^{3/2}$

REFERENCES

No.	Author	Title, etc
1	J. Weber C. King	Analysis of the zero-lift wave drag measured on delta wings. RAE Technical Report 76072 (1976)
2	L.C. Squire	The use of excess engine exit area over intake area to reduce zero-lift drag at high supersonic speeds. Aeronautical Quarterly, Vol.XVII, pp 260-274 (1965)
3	W.T. Lord G.G. Brebner	Supersonic flow past slender pointed wings with 'similar' cross sections at zero lift. Aeronautical Quarterly, Vol.X, pp 79-102 (1959)
4	L.C. Squire	Applications of shock expansion theory to the flow over non-conical delta wings. Aeronautical Journal, Vol.76, 659-662 (1972)
5	R. Hillier	Three-dimensional wings in hypersonic flow. Jour. Fluid Mechanics, Vol.54, pp 305-337 (1972)
6	D. Küchemann	Hypersonic aircraft and their aerodynamic problems. Progress in Aeronautical Sciences, Vol.6, pp 271-353 (1965)
7	D. Küchemann J. Weber	An analysis of some performance aspects of various types of aircraft designed to fly over different ranges at different speeds. Progress in Aeronautical Sciences, Vol.9, pp 329-455 (1968)
8	J.G. Jones K.C. Moore J. Pike P.L. Roe	A method for designing lifting configurations for high supersonic speeds using axisymmetric flow fields. Ingenieur-Archiv 37 Band 1, pp 56-72 (1968)
9	J. Pike	On conical waveriders. RAE Technical Report 70090 (1970)
10	L.C. Squire	Pressure distributions and flow patterns on some conical shapes with sharp leading edges and symmetrical cross-sections at M = 4.0. ARC R&M 3340 (1962)
11	L.C. Squire	Pressure distributions and flow patterns at M = 4 on some delta wings. ARC R&M 3373 (1963)

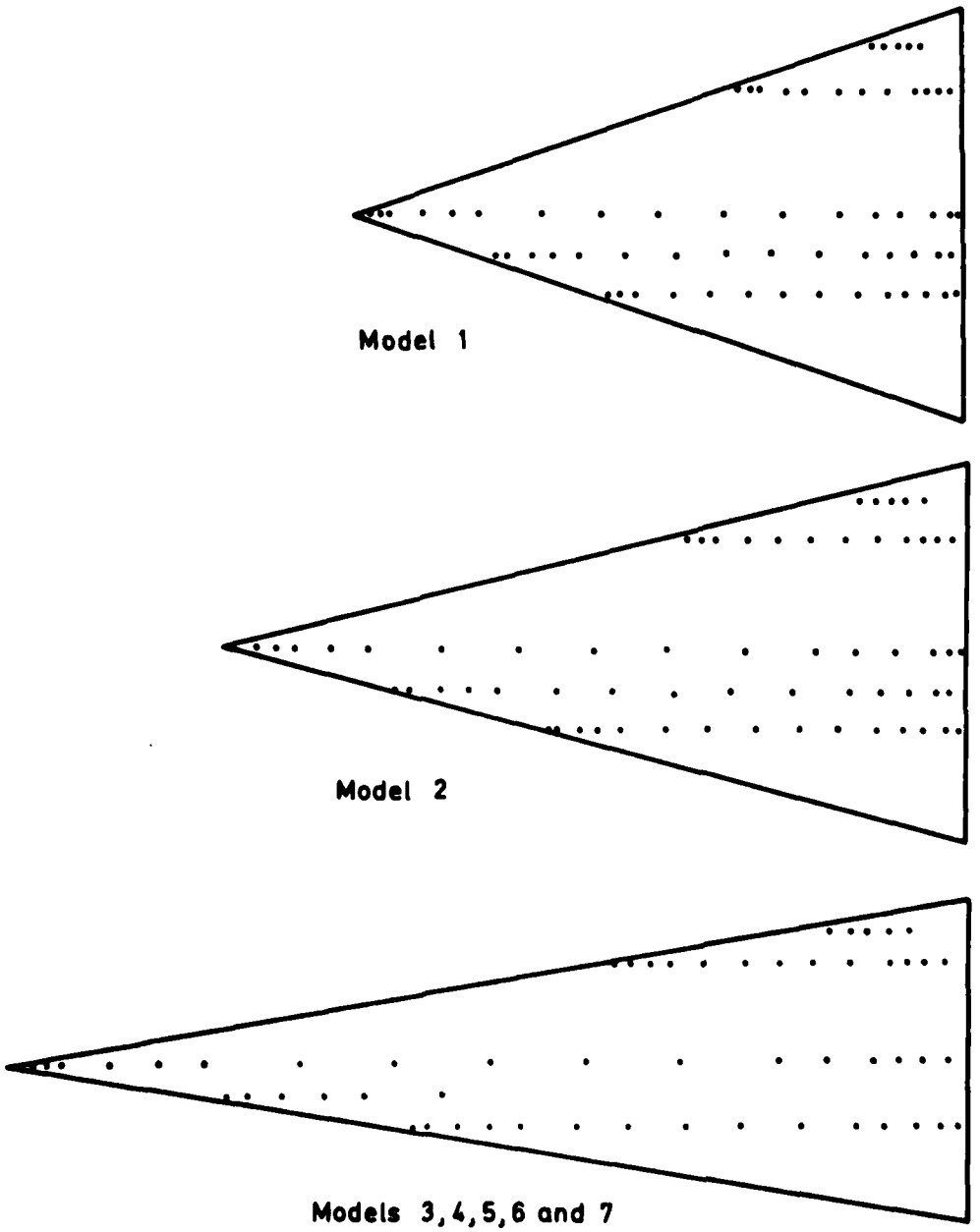

Fig 1 Planforms and pressure hole positions

Fig 2

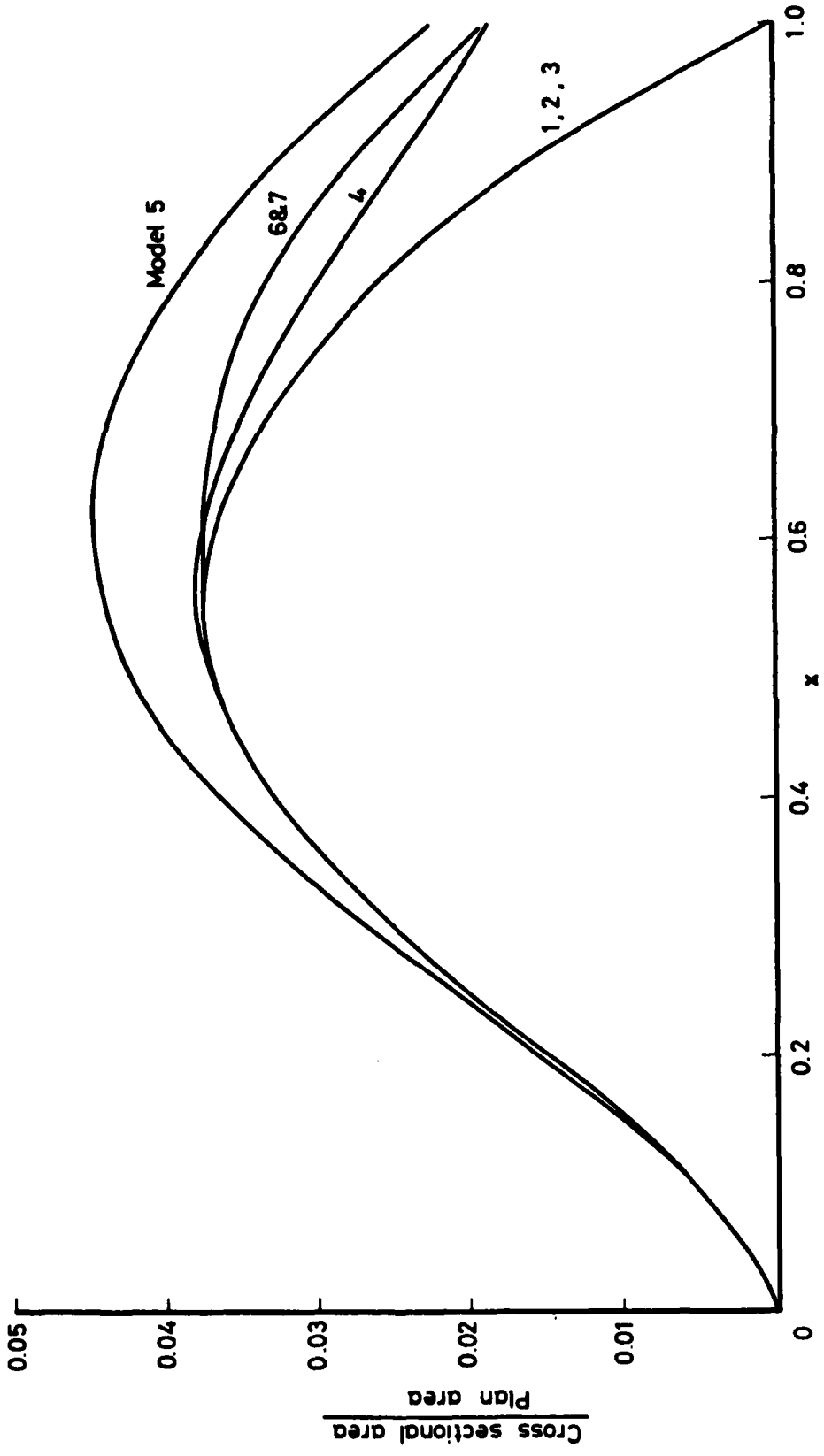

Fig 2 Longitudinal distributions of cross-sectional area

TR 80038

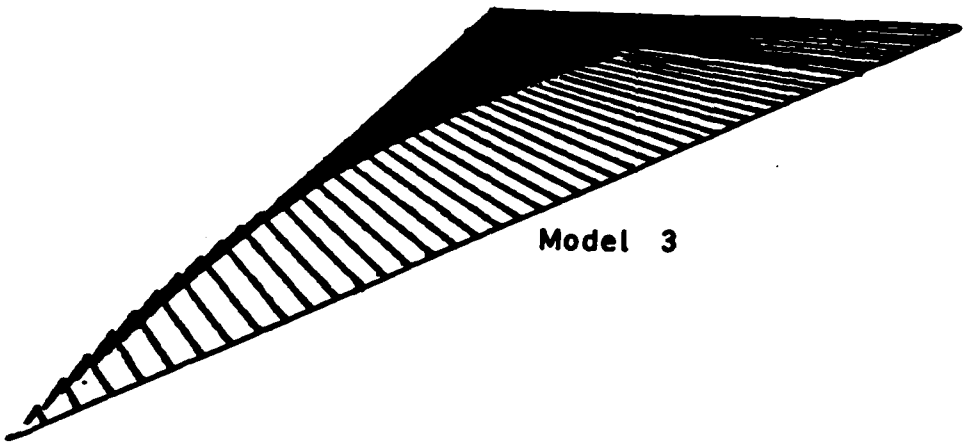

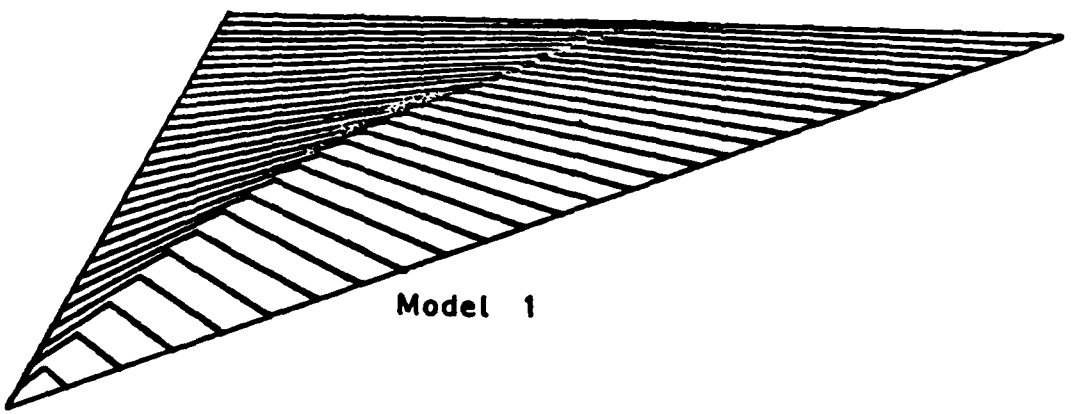

Fig 3 Cross sections, shown in perspective, for two of the basic wings

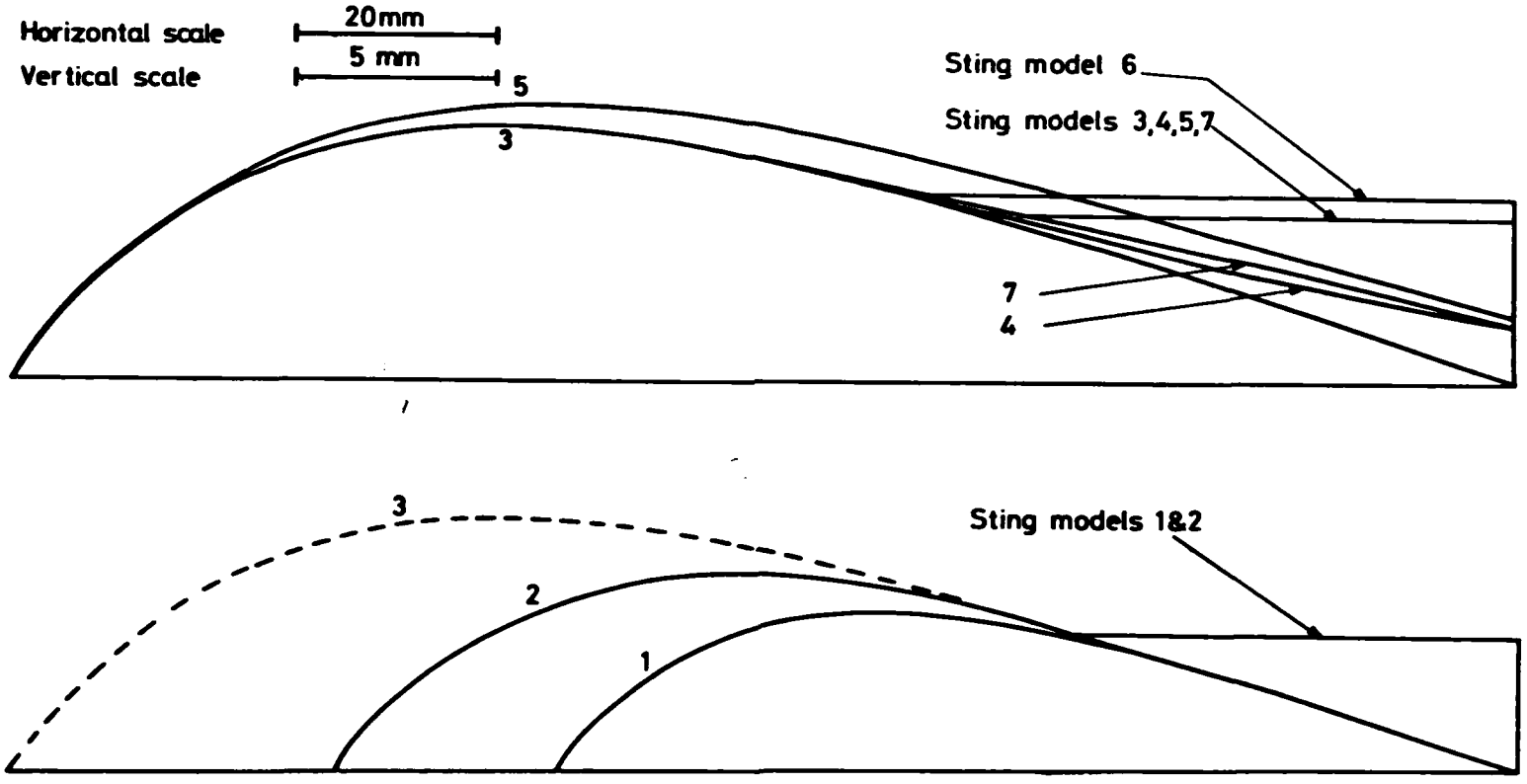

Fig 4 Centre sections

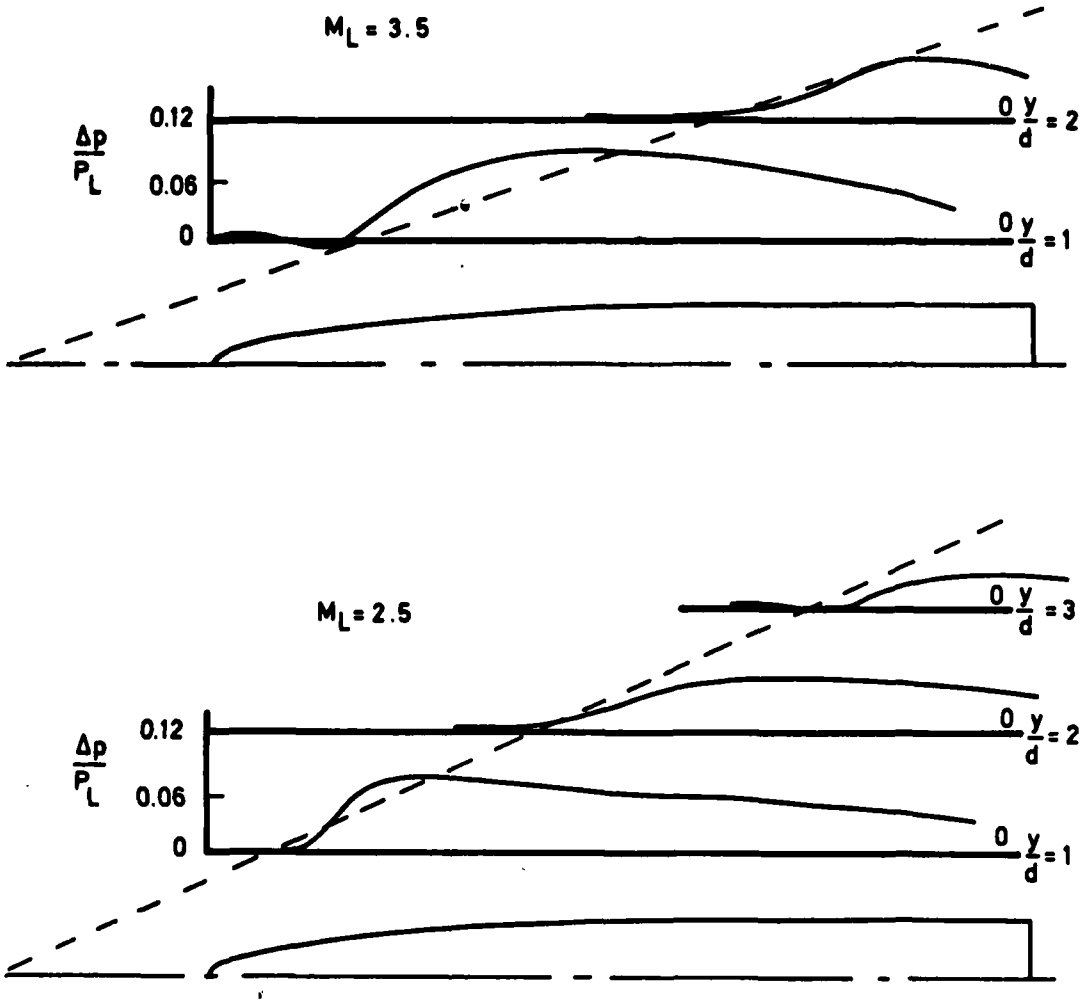

TR 80068

Fig 5 Shield interference pressures

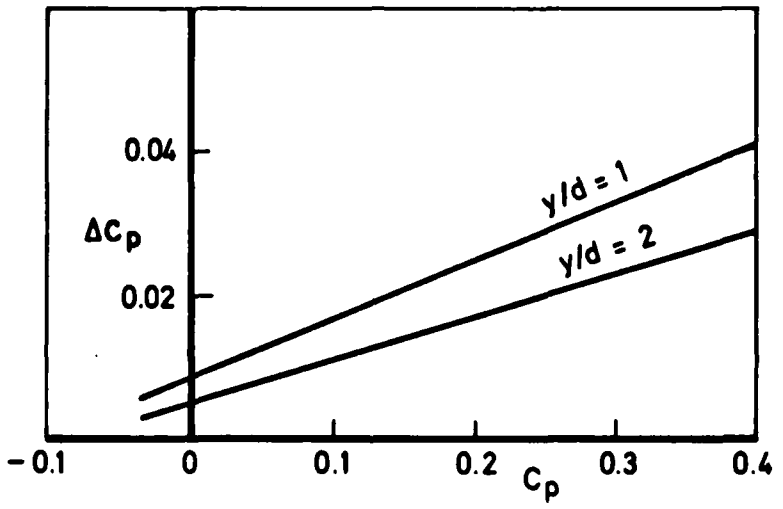

Fig 6 Maximum values of sting-interference pressure, extrapolated to $M_\infty = 3.96$

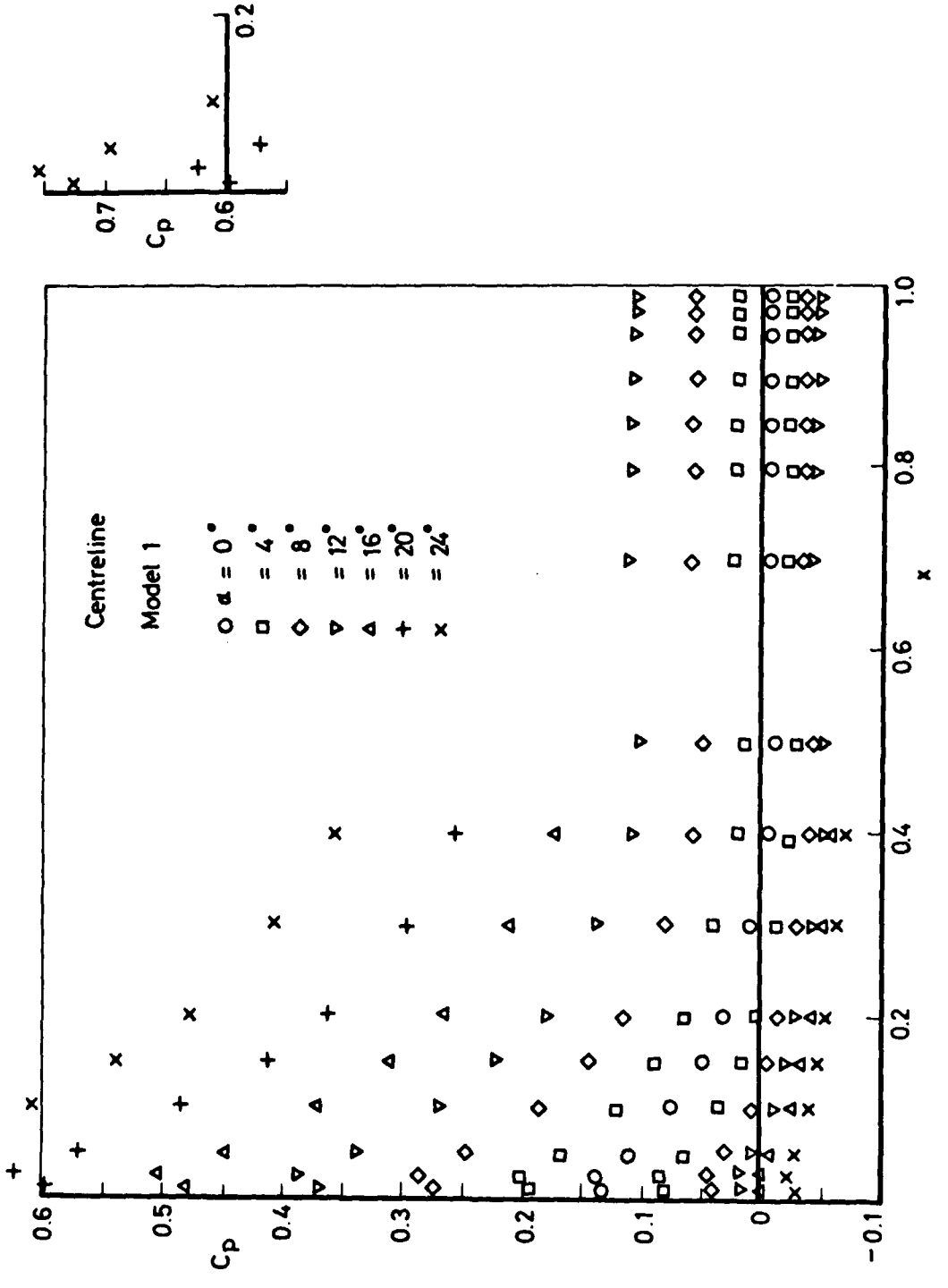

Fig 7a Pressure distributions on model 1, centre line

Fig 7b

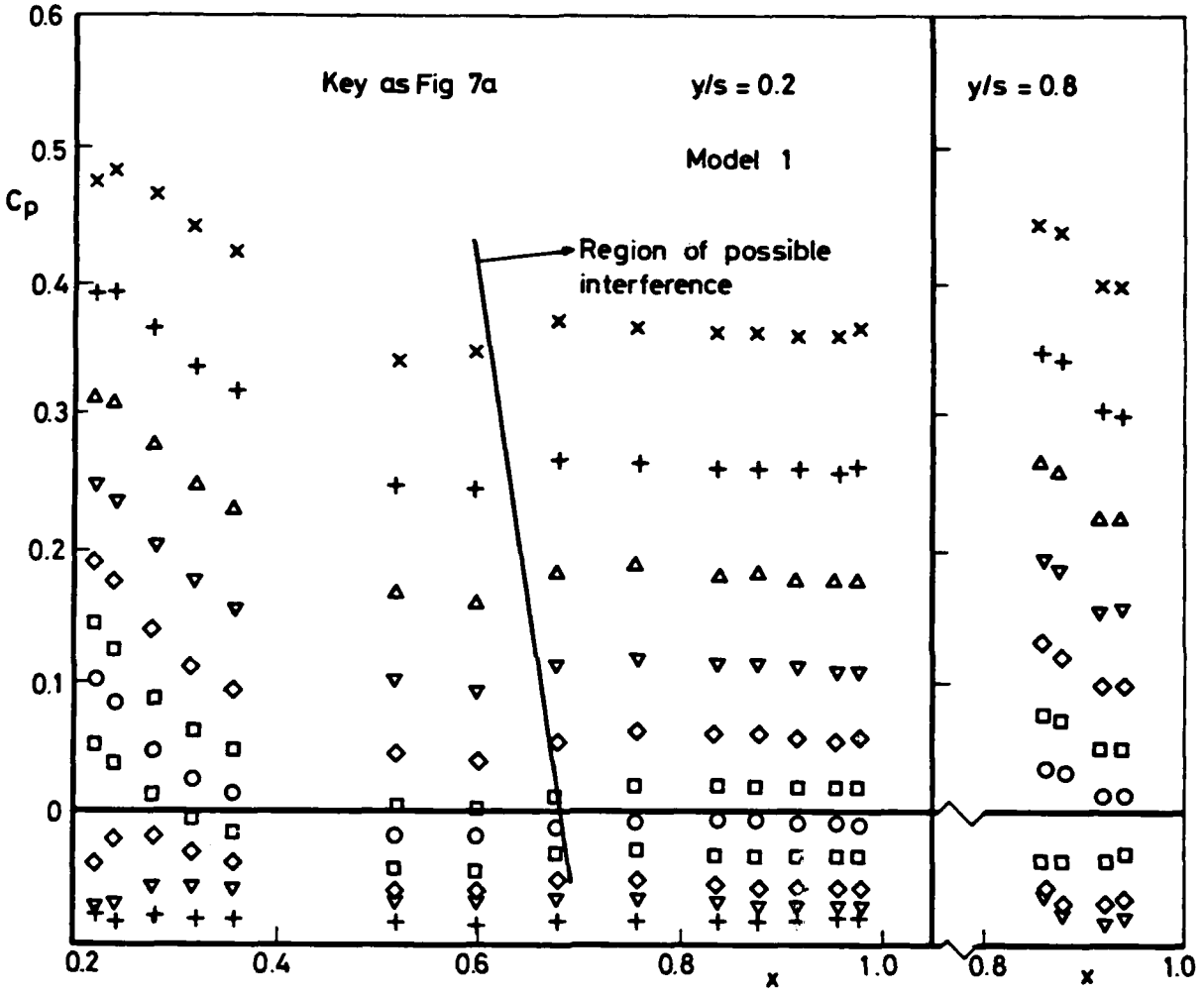

Fig 7b Pressure distributions on model 1, y/s = 0.2, 0.8

TR.80068

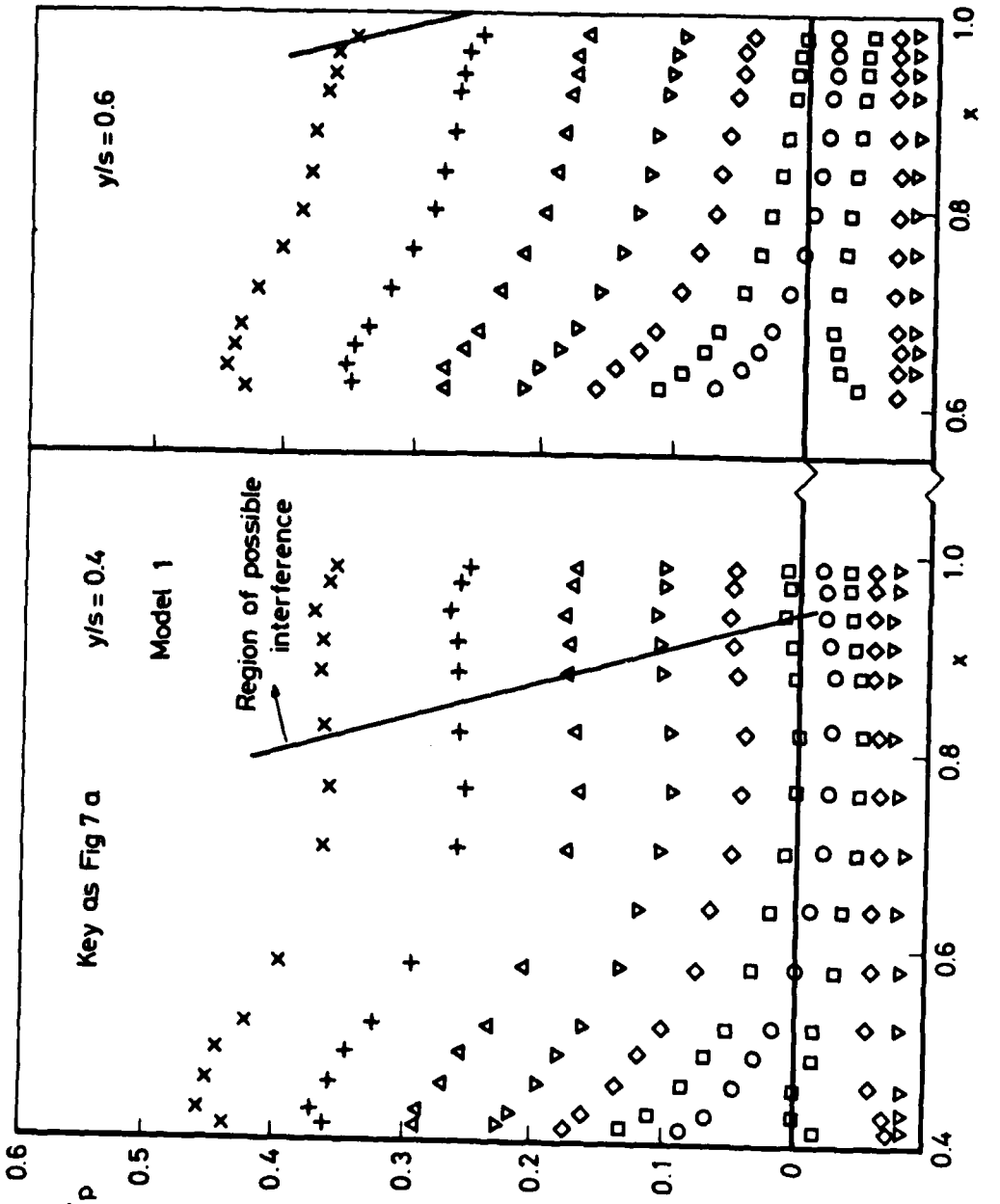

Fig 7c Pressure distributions on model 1, y/s = 0.4, 0.6

Fig 8a

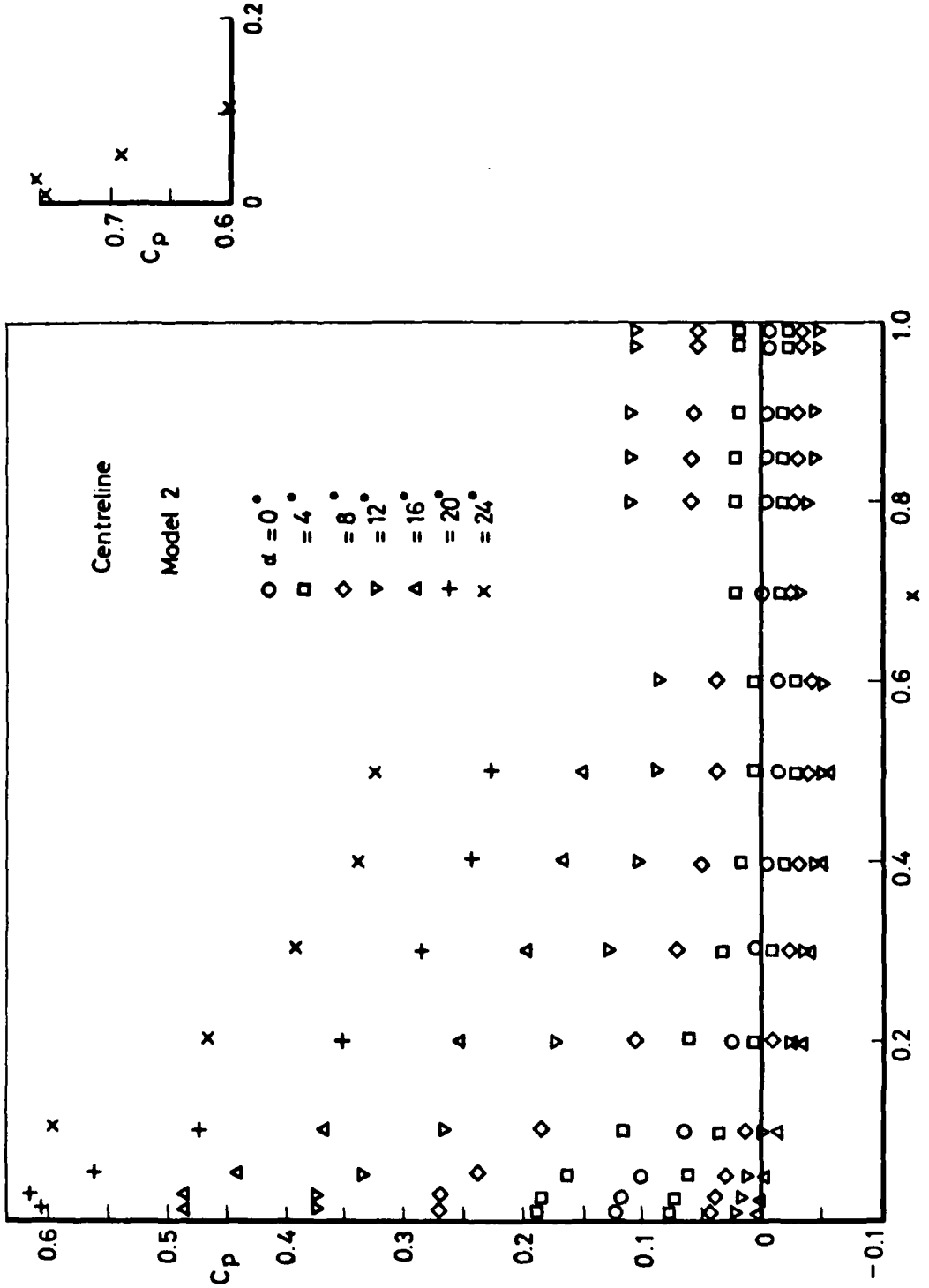

Fig 8a Pressure distributions on model 2, centre line

TR 80068

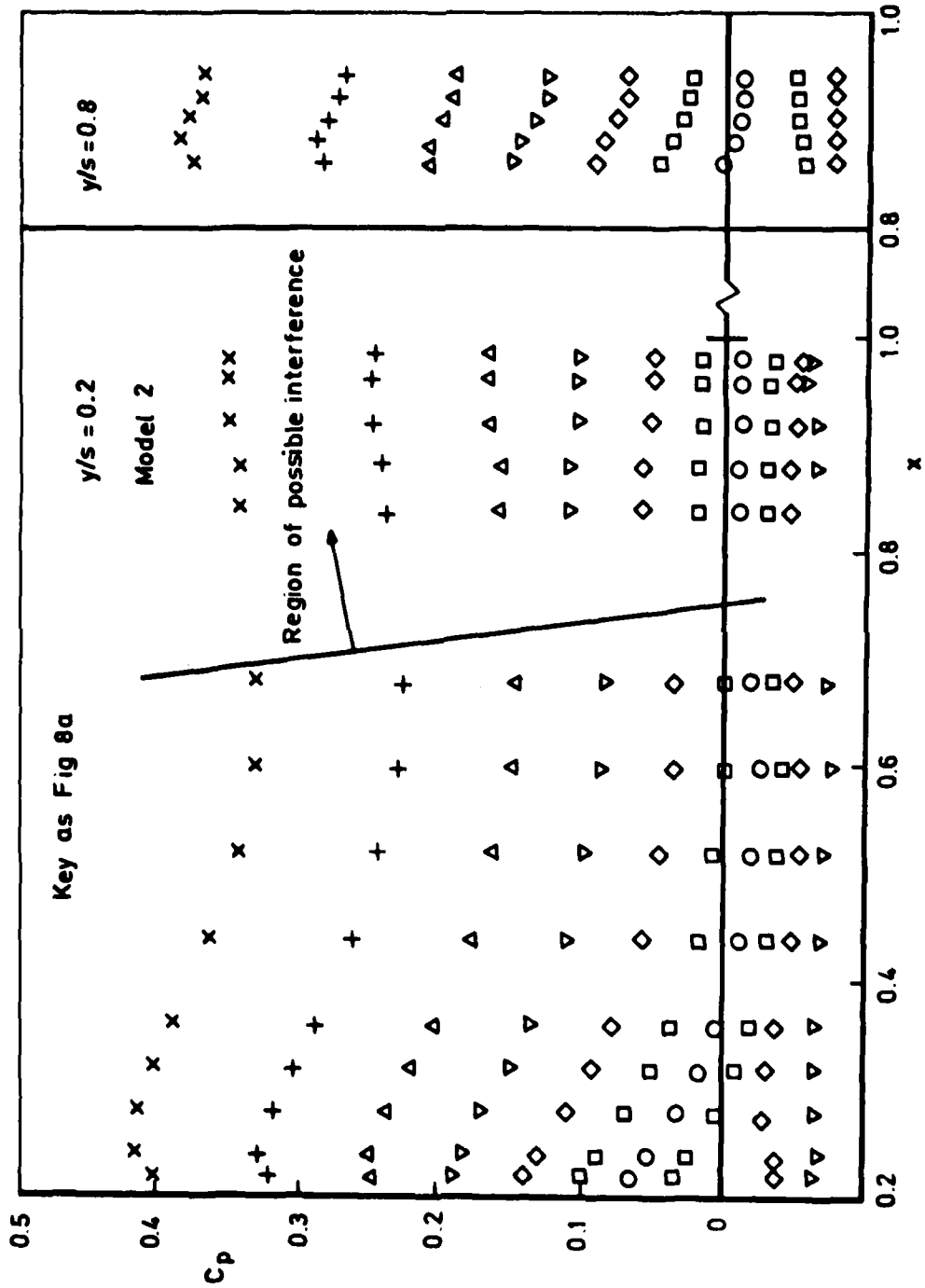

Fig 8b Pressure distributions on model 2, y/s = 0.2, 0.8

Fig 8c

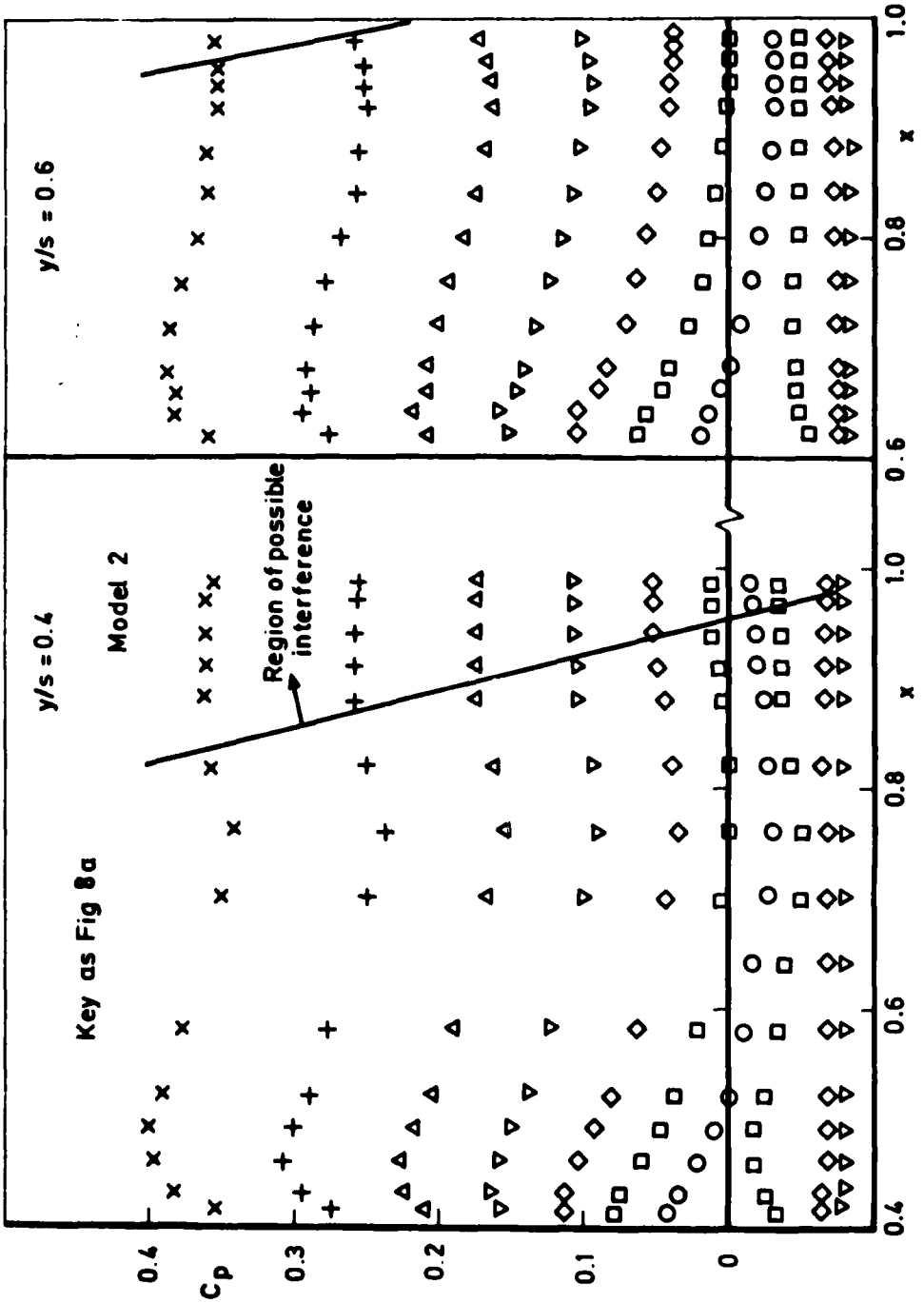

Fig 8c Pressure distributions on model 2, y/s = 0.4, 0.6

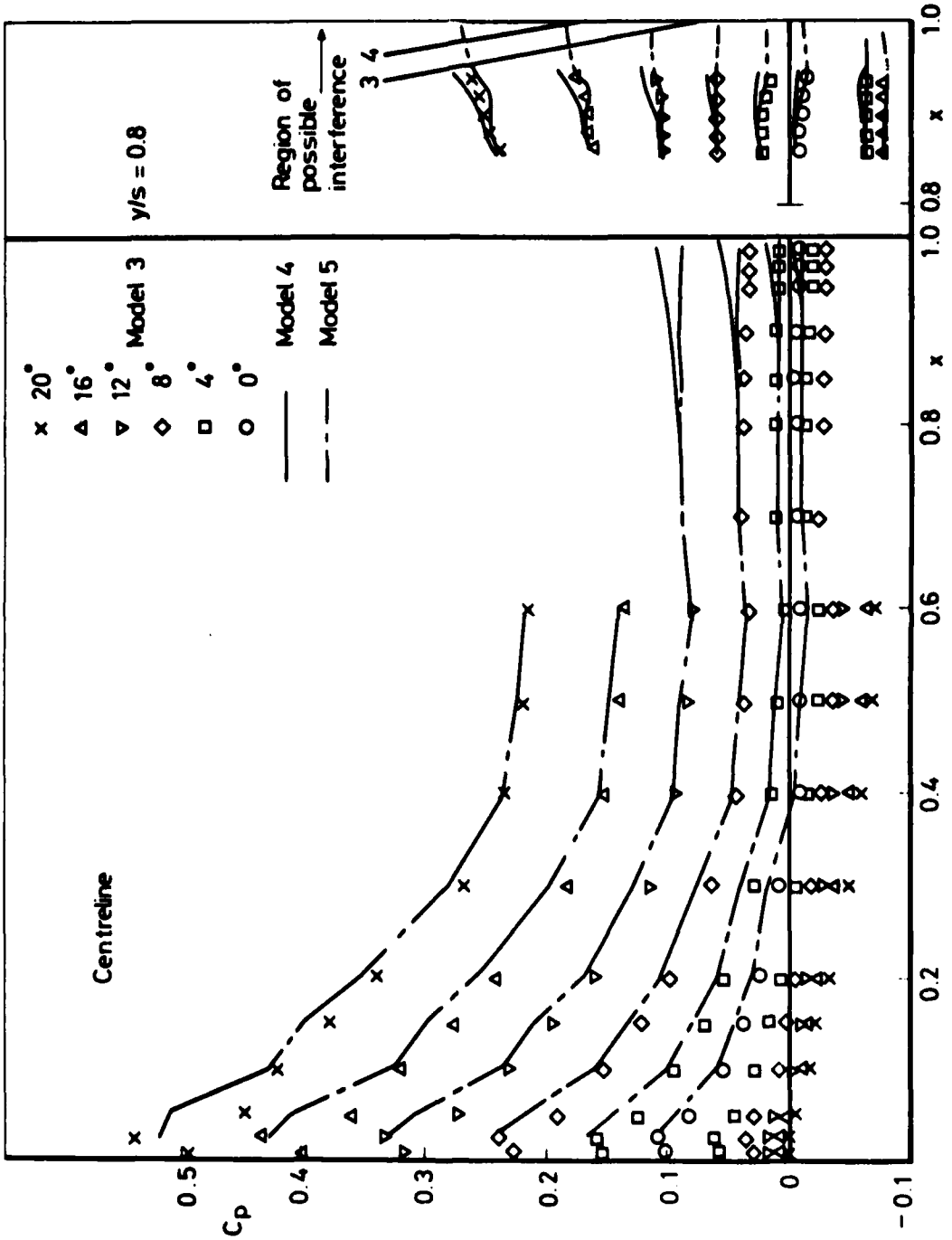

Fig 9a Pressure distributions on models 3, 4, 5, centre line and y/s = 0.8

Fig 9b

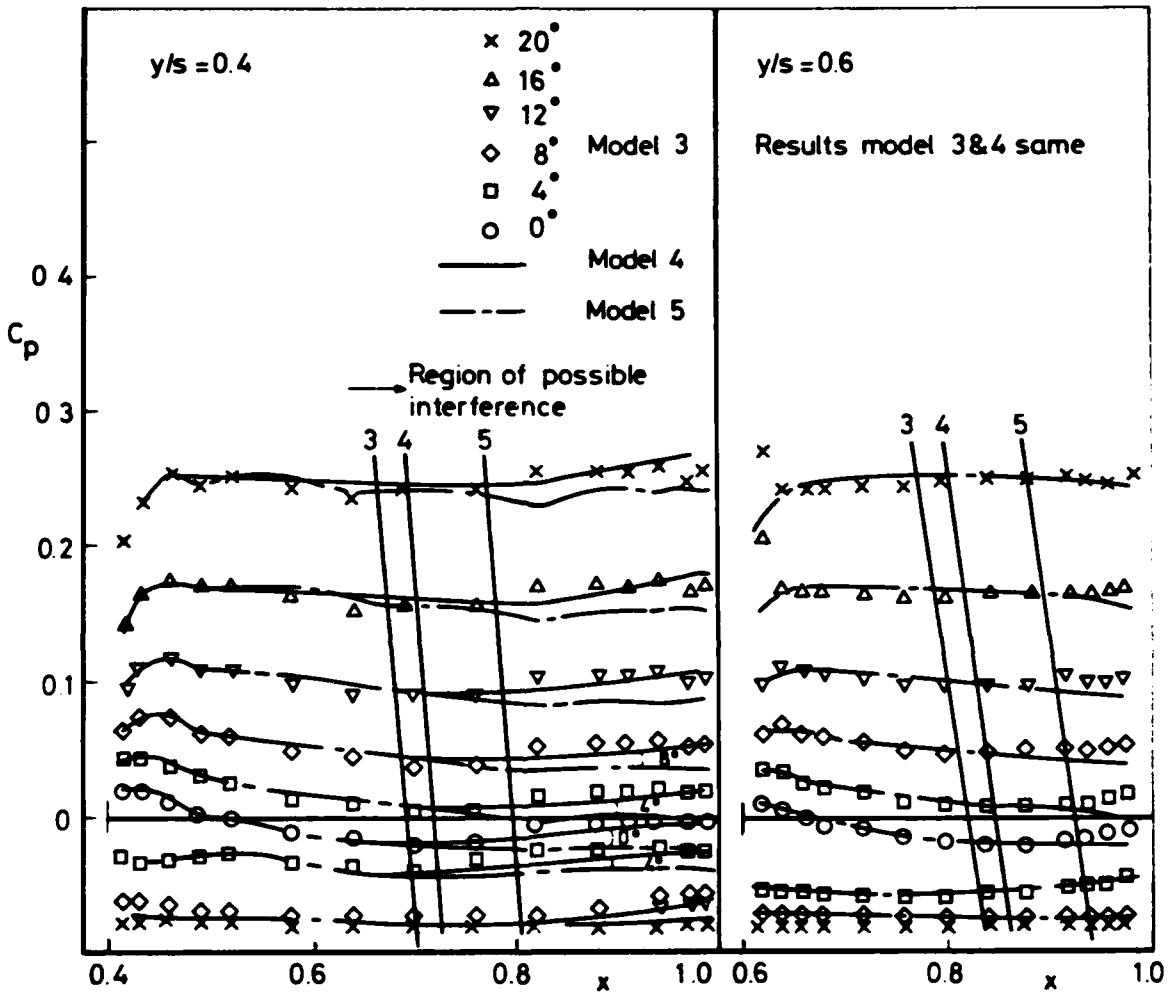

Fig 9b Pressure distributions on models 3, 4, 5, y/s = 0.4, 0.6

TR 80068

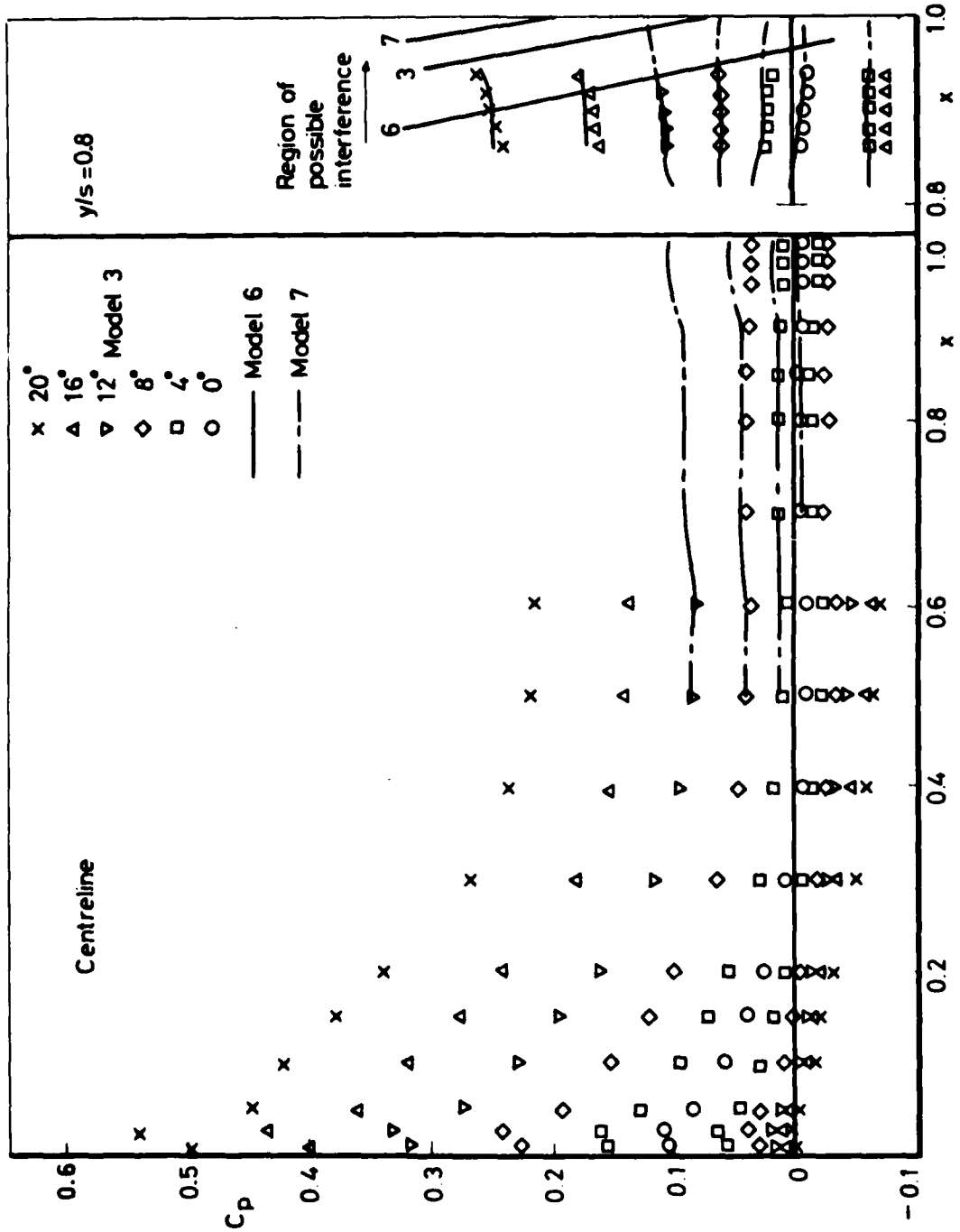

Fig 10a Pressure distributions on models 3, 6, 7, centre line and y/s = 0.8

Fig 10b

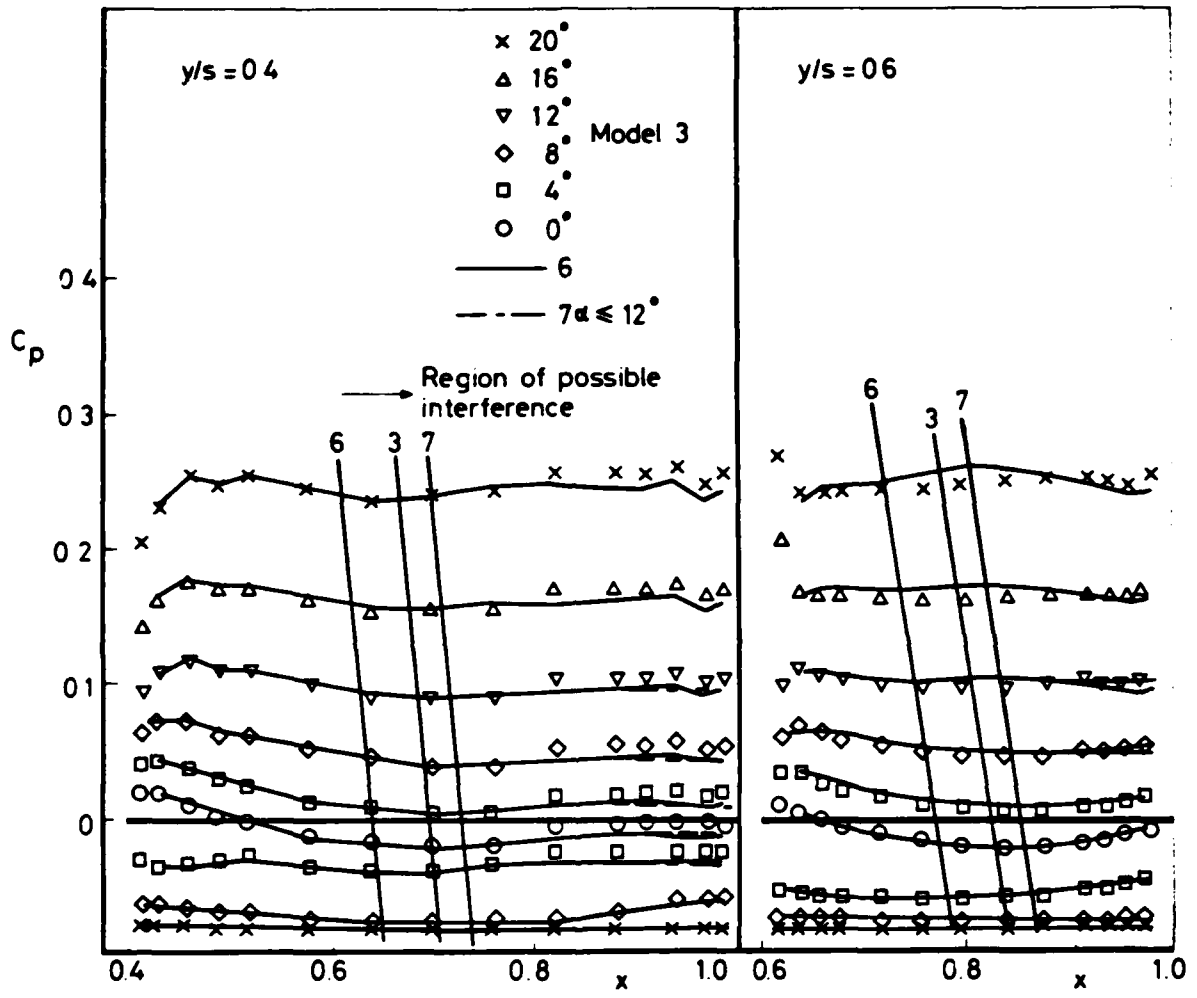

Fig 10b Pressure distributions on models 3, 6, 7, y/s = 0.4, 0.6

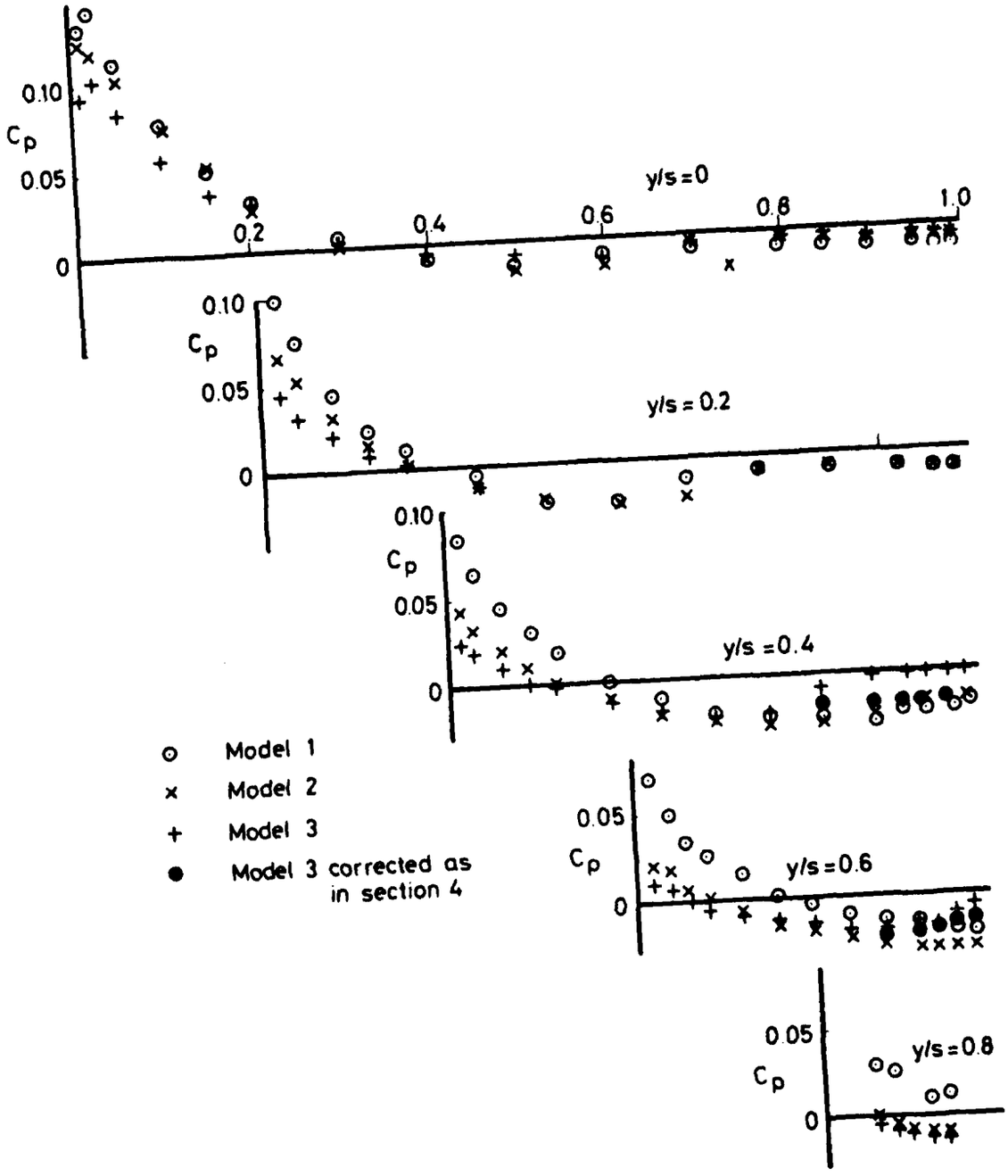

TR 80068

Fig 11 Pressure distributions at zero incidence, models 1, 2, 3

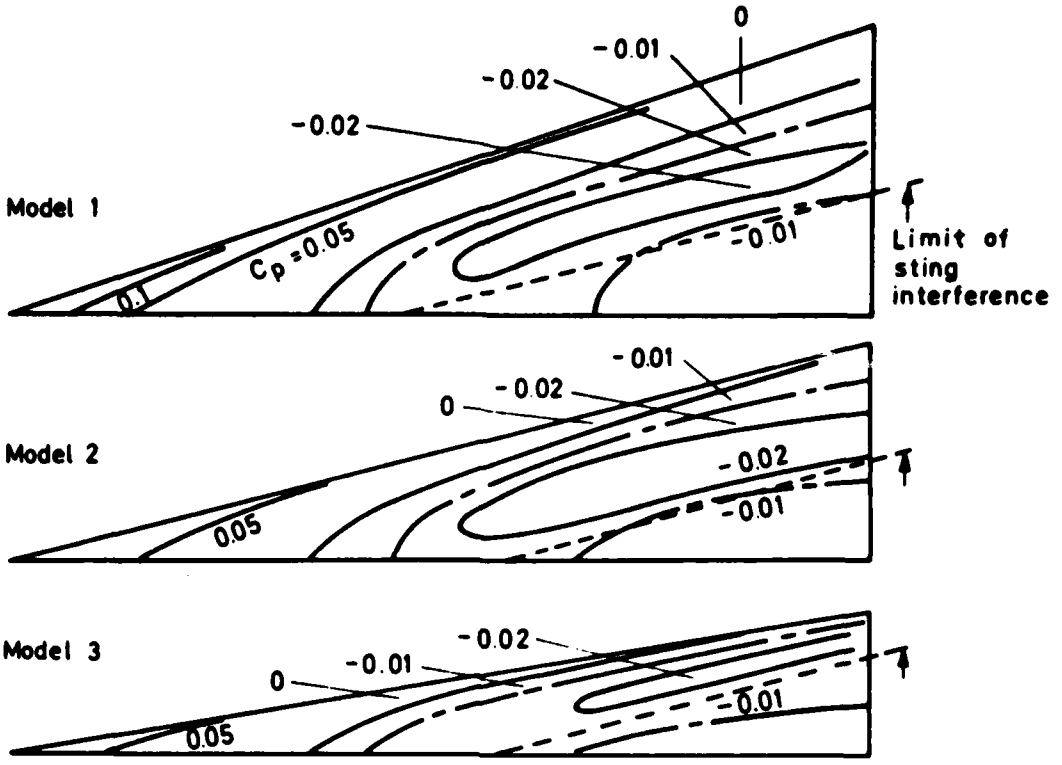

Fig 12 Pressure contours, models 1, 2, 3

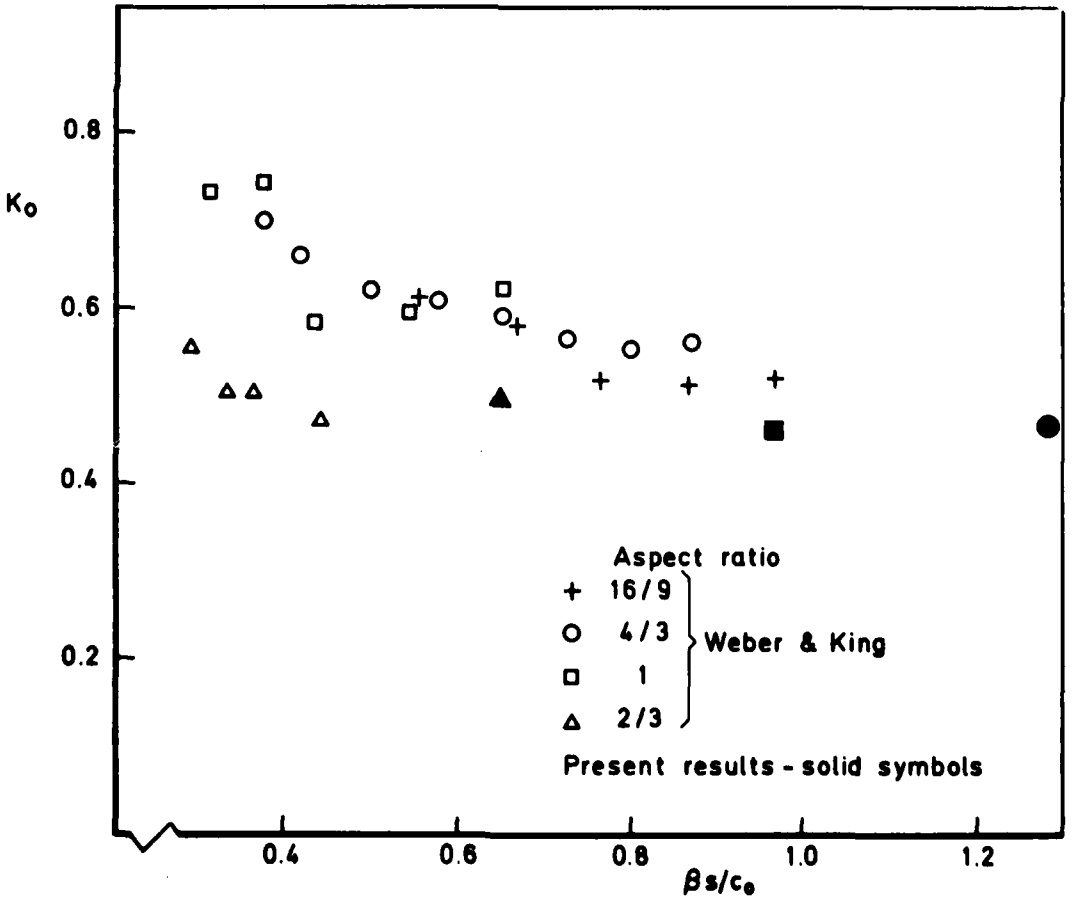

Fig 13 Variation of K_0 with $\beta s/c_0$

TR 80068

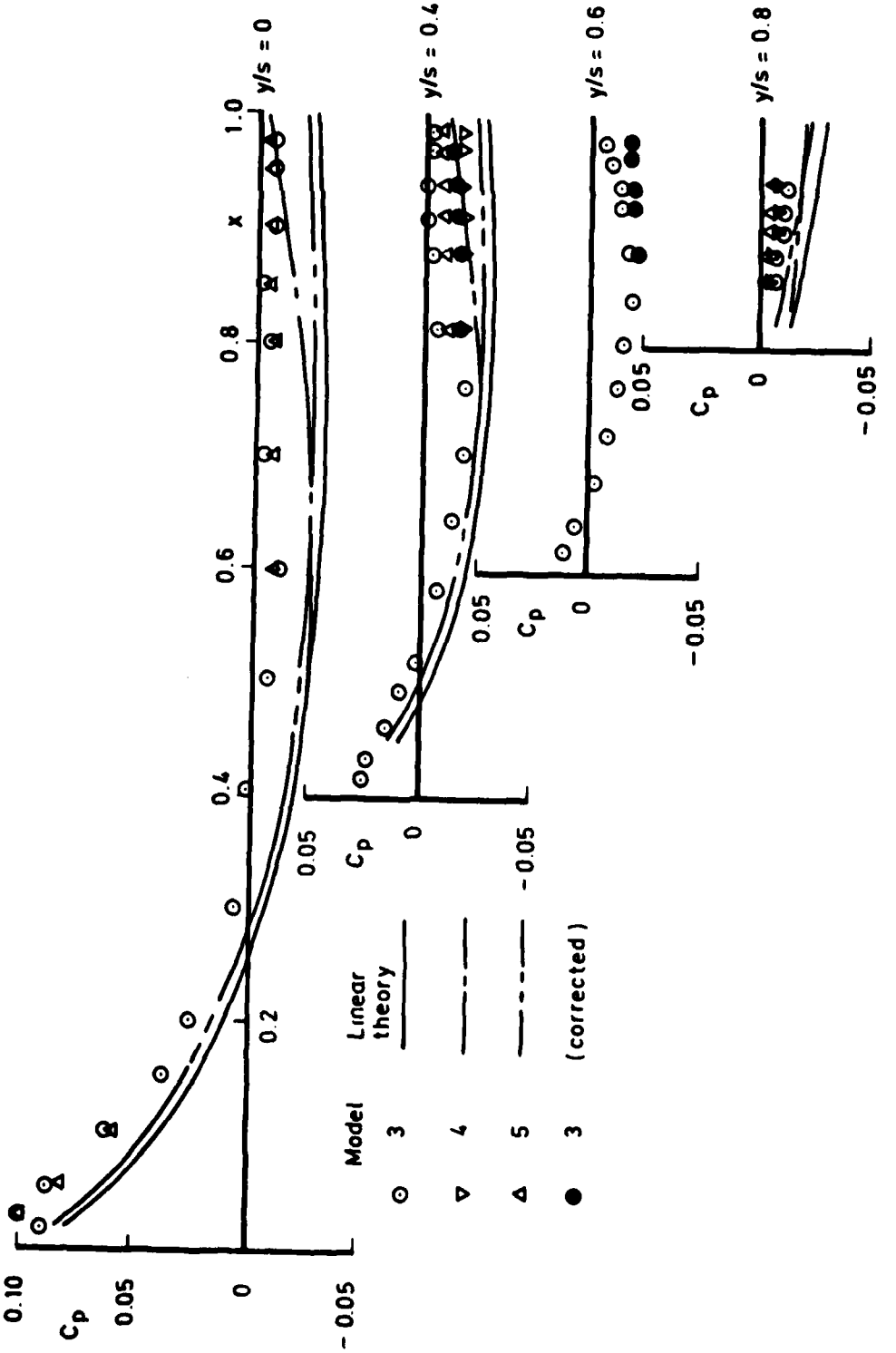

Fig 14 Pressure distributions at zero incidence, models 3, 4, 5

Fig 15

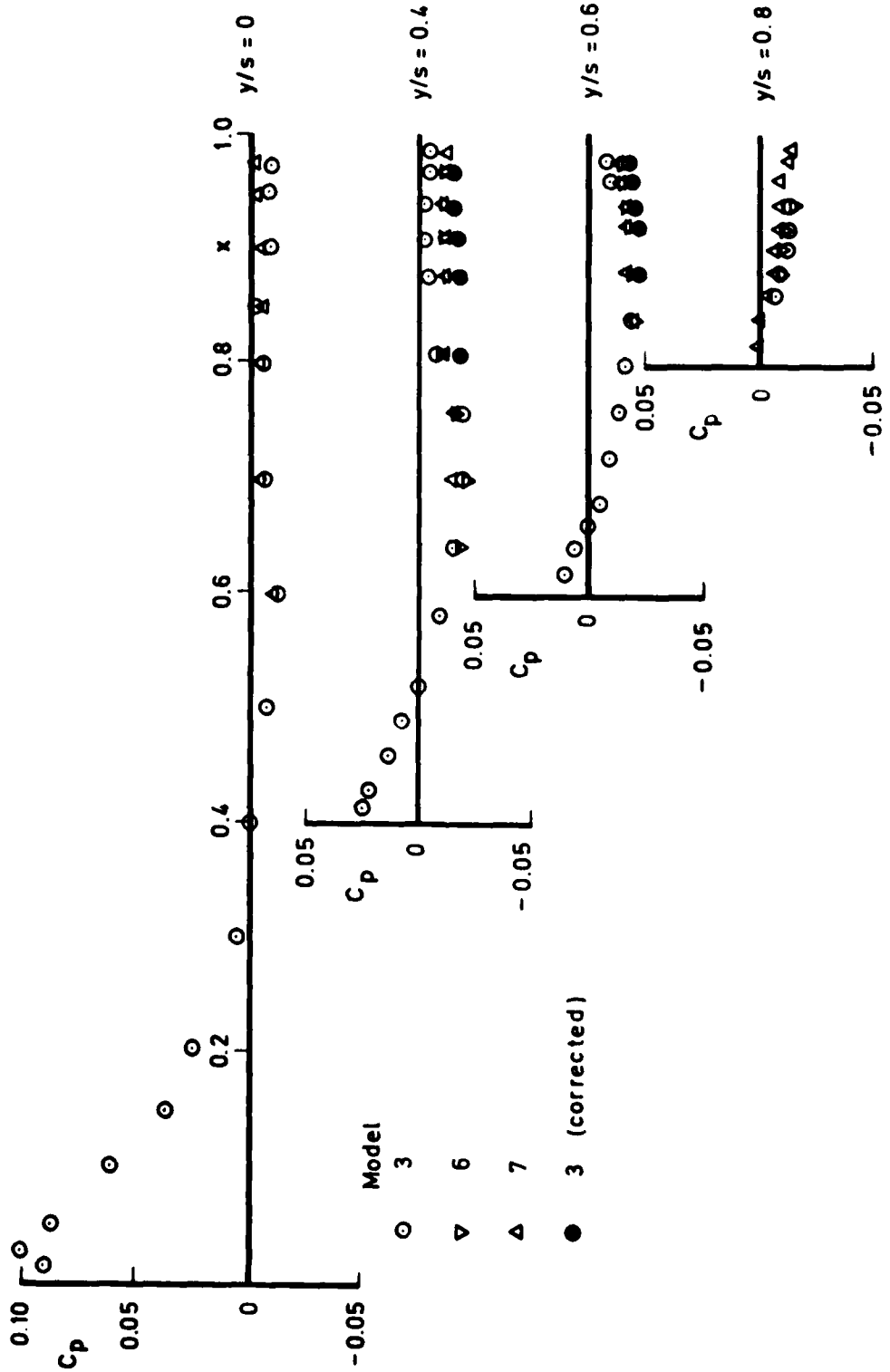

Fig 15 Pressure distributions at zero incidence, models 3, 6, 7

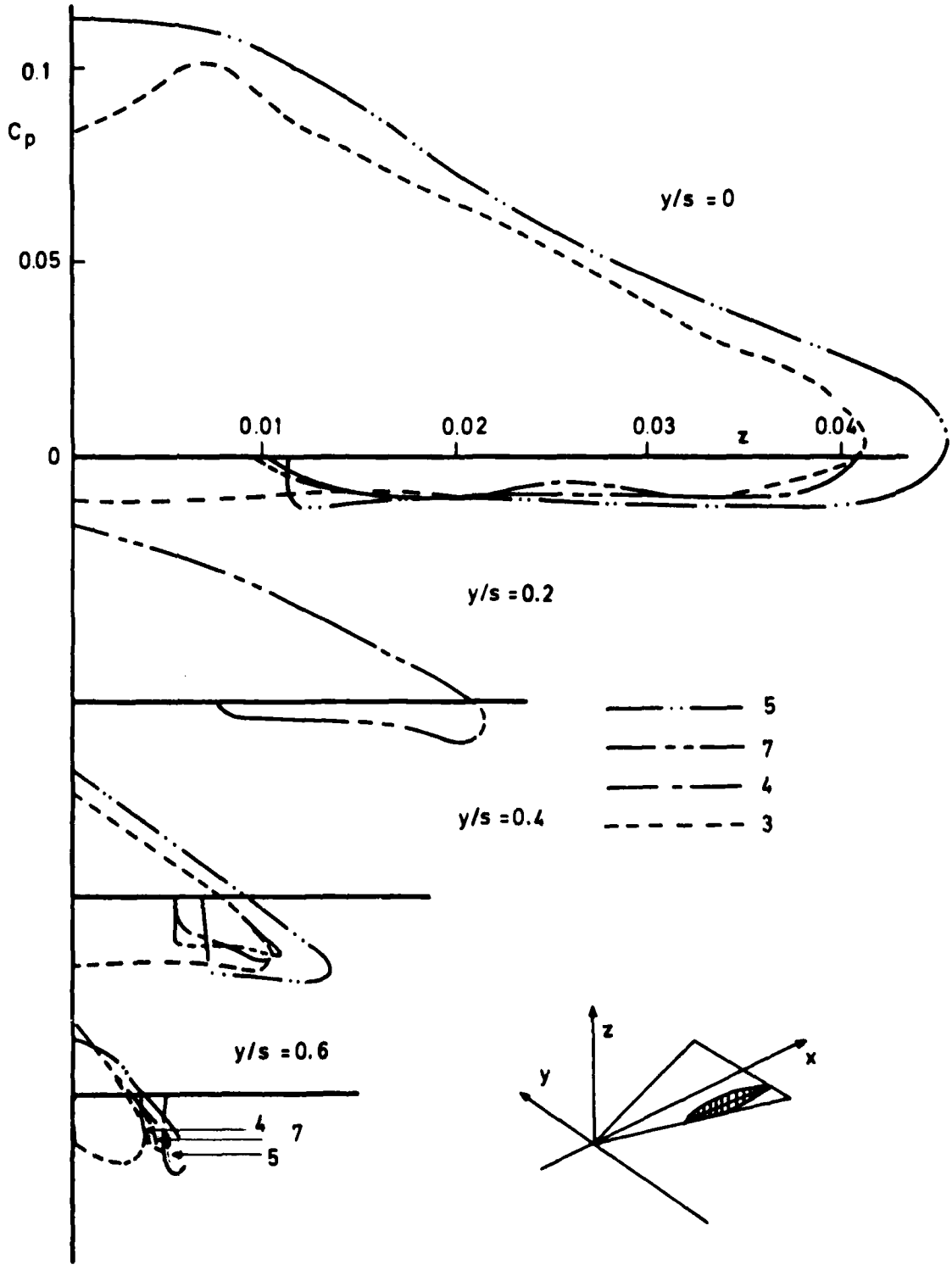

TR 80068

Fig 16 Drag loops, models 3, 4, 5, 7

Fig 17

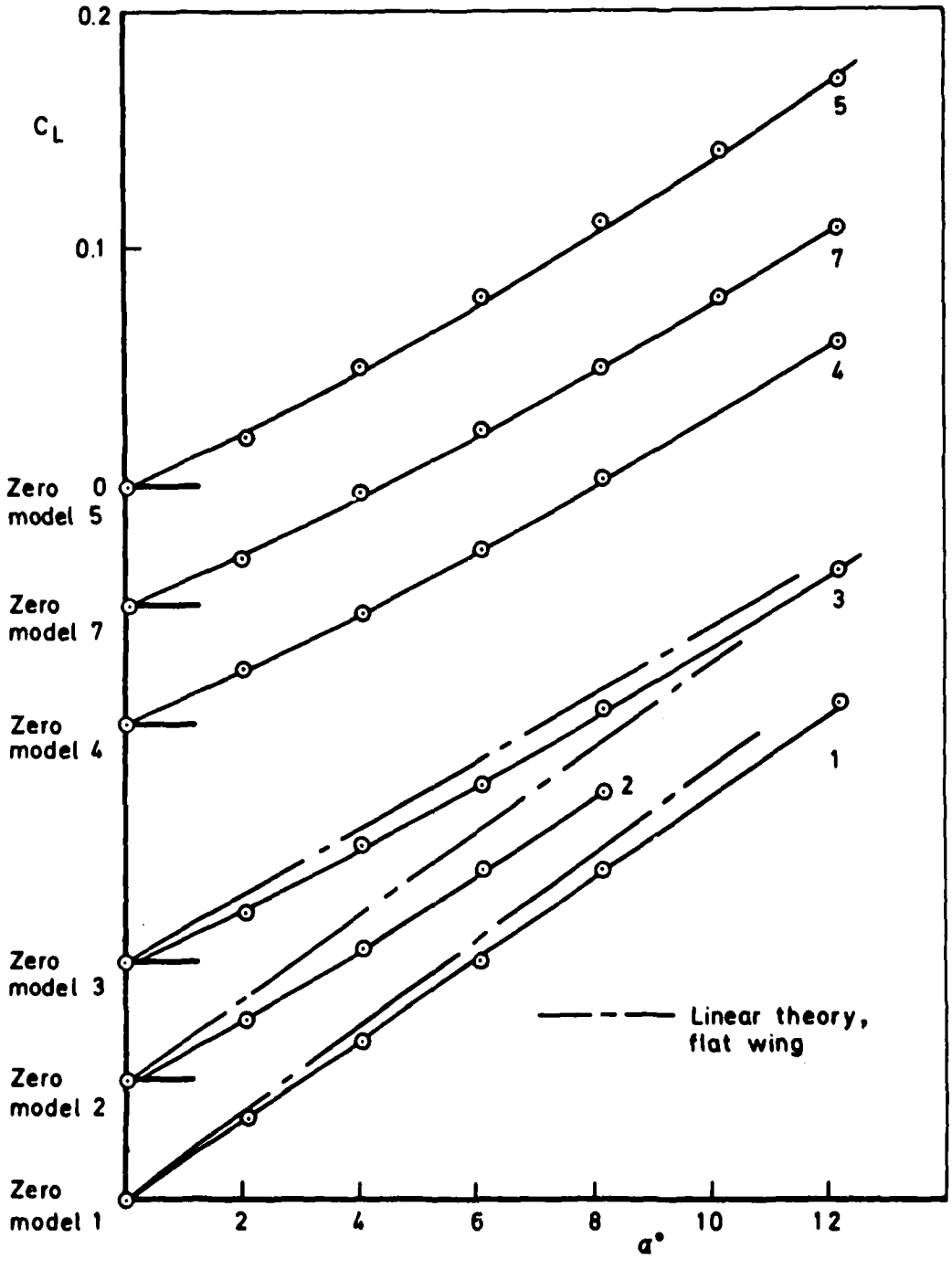

TR 80068

Fig 17 Variation of C_L with α

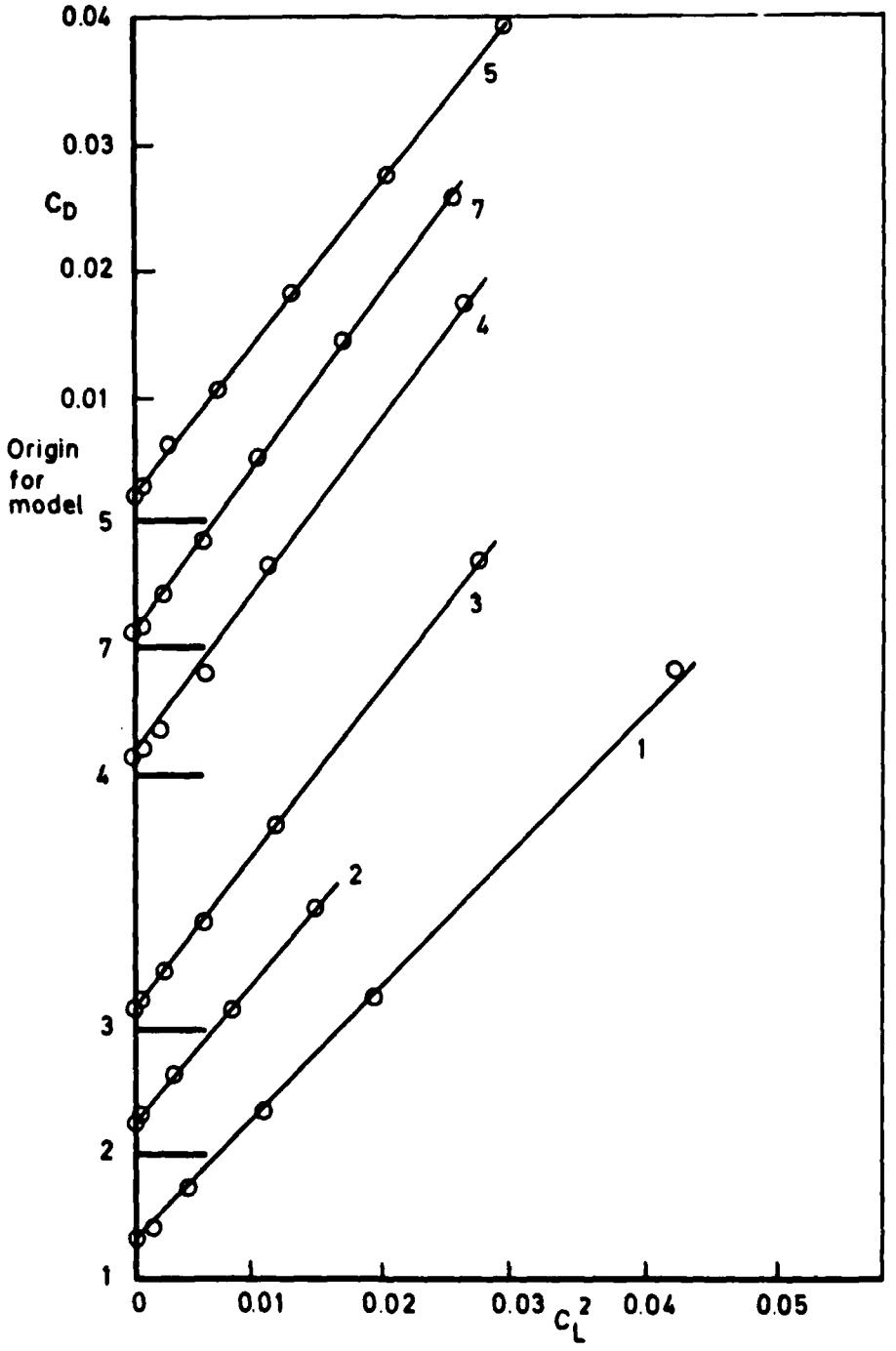

TR 80068

Fig 18 Variation of C_D with C_L^2

Fig 19

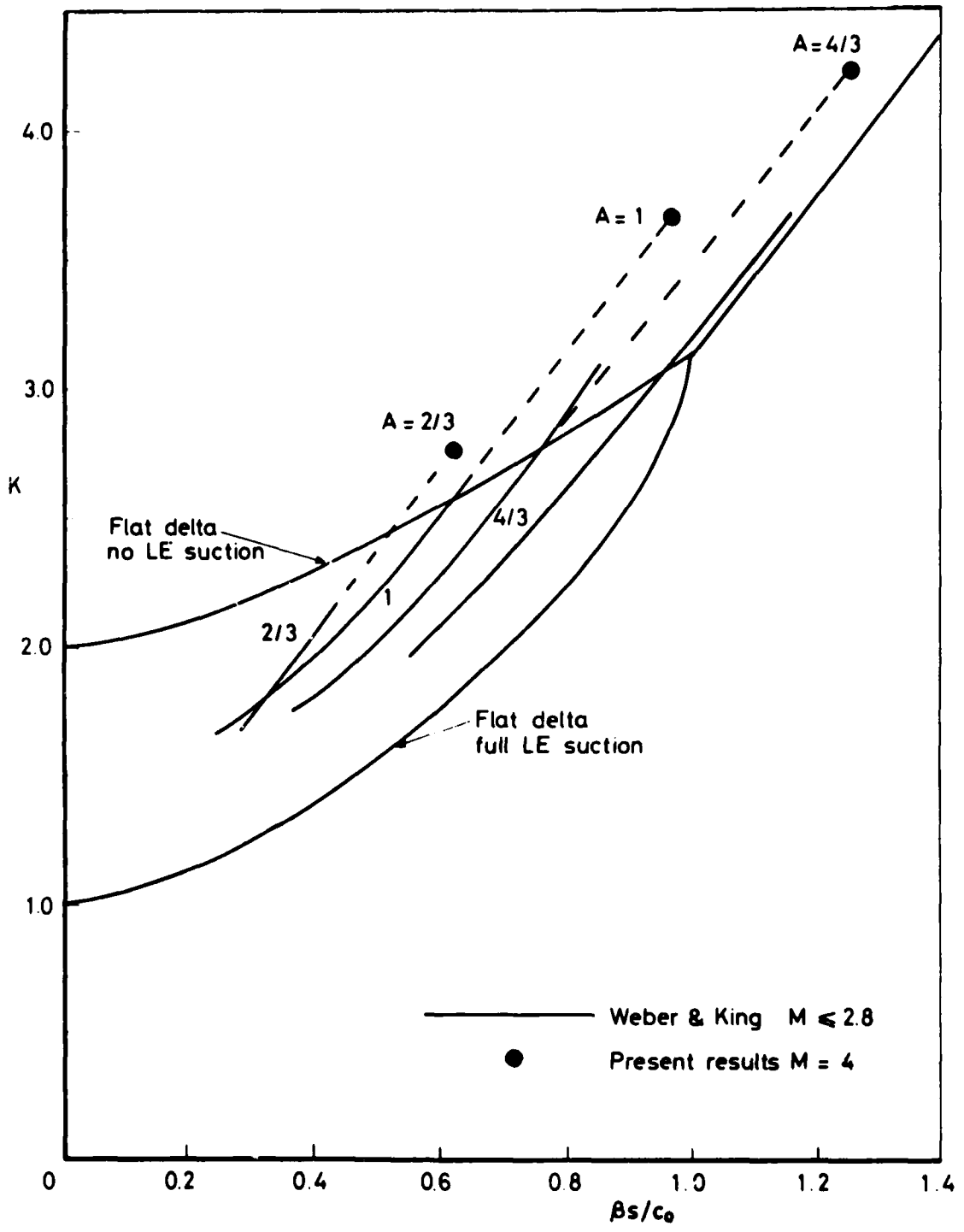

TR 80068

Fig 19 Lift-dependent drag factors

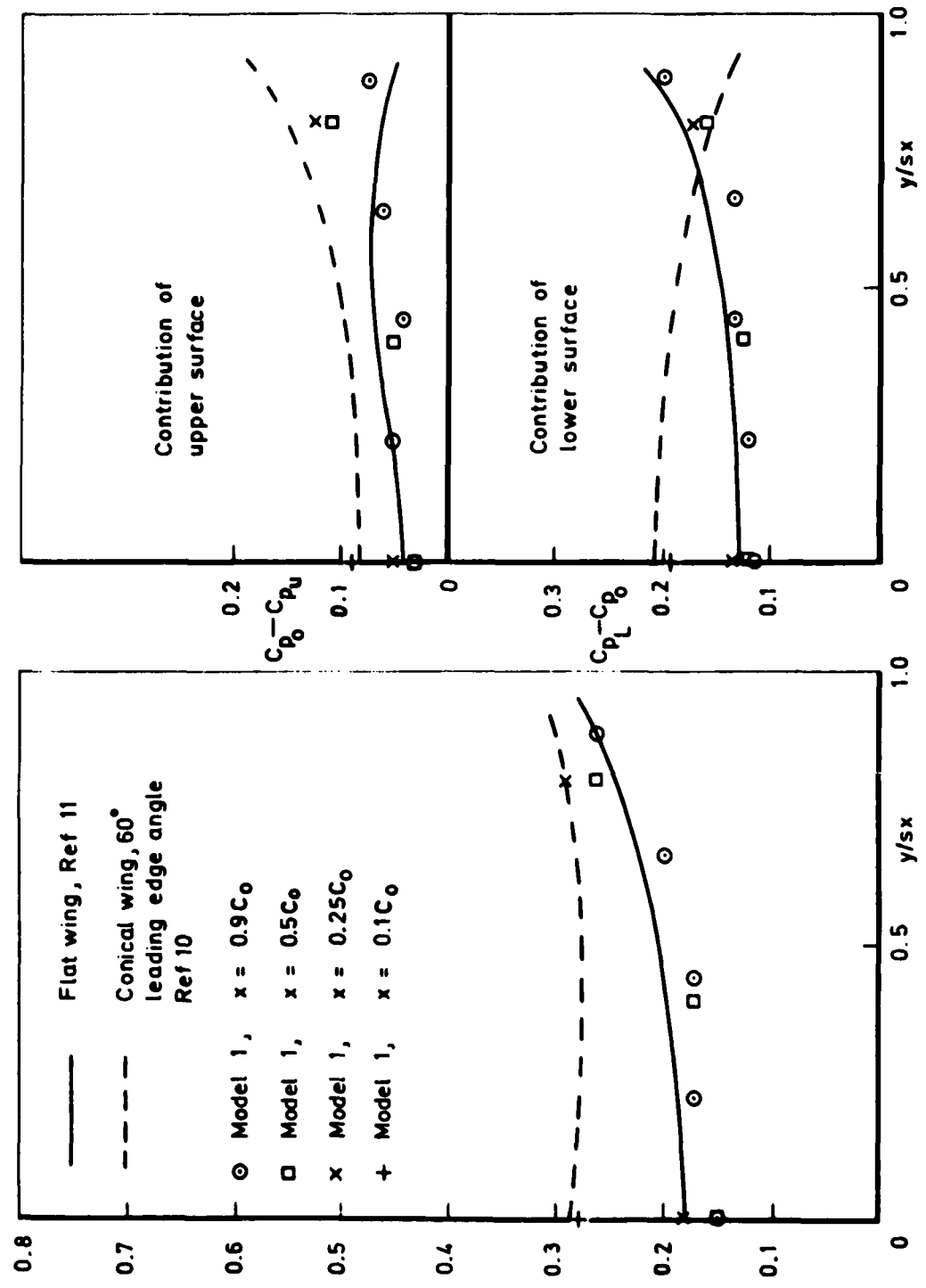

Fig 20 Lifting pressures: model 1 at $\alpha = 12°$

Fig 21

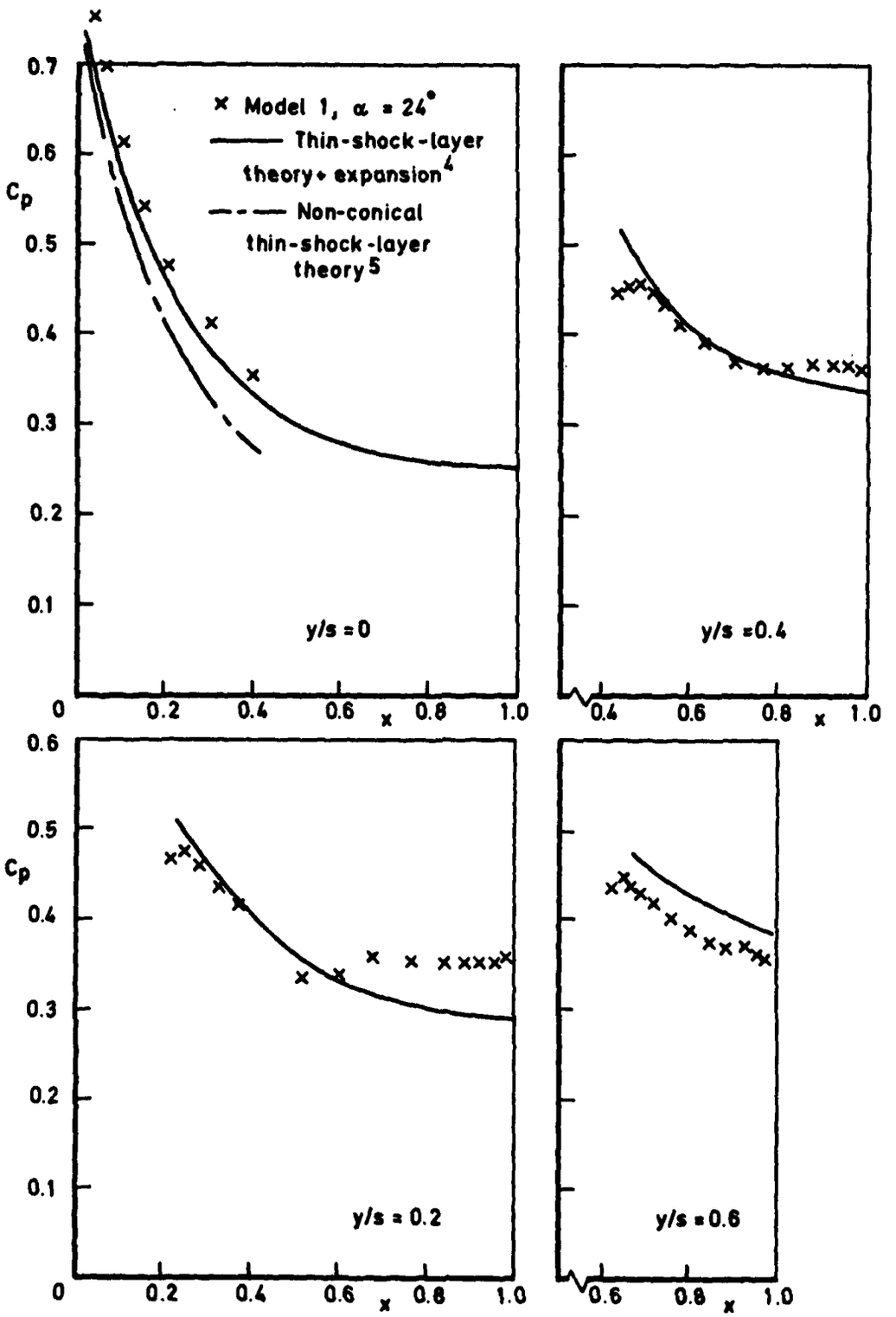

TR 80058

Fig 21 Comparison with theory, model 1

Overall security classification of this page

UNLIMITED

As far as possible this page should contain only unclassified information. If it is necessary to enter classified information, the box above must be marked to indicate the classification, e.g. Restricted, Confidential or Secret.

1. DRIC Reference (to be added by DRIC)	2. Originator's Reference	3. Agency Reference	4. Report Security Classification/Marking
	RAE TR 80068	N/A	UNLIMITED

5. DRIC Code for Originator	6. Originator (Corporate Author) Name and Location
7673000W	Royal Aircraft Establishment, Farnborough, Hants, UK
5a. Sponsoring Agency's Code	**6a. Sponsoring Agency (Contract Authority) Name and Location**
N/A	N/A

7. Title

Pressure distributions on some delta wings at M = 4

7a. (For Translations) Title in Foreign Language

7b. (For Conference Papers) Title, Place and Date of Conference

8. Author 1. Surname, Initials	9a. Author 2	9b. Authors 3, 4	10. Date	Pages	Refs.
Squire, L.C.	Moore, K.C.		May 1980	44	11

11. Contract Number	12. Period	13. Project	14. Other Reference Nos.
N/A	N/A		Aero 3484

15. Distribution statement

(a) Controlled by – Unlimited

(b) Special limitations (if any) –

16. Descriptors (Keywords) (Descriptors marked * are selected from TEST)

Slender wings. Wave drag*. Supersonic aircraft*.

17. Abstract

Complete pressure distributions are presented for a series of delta wings tested through an incidence range at a Mach number of 4. The results have been integrated to obtain lift and drag coefficients and the values found are in good agreement with the trend from measurements on similar wings at lower Mach numbers. Some of the models were designed to test a possible method of engine/airframe integration. The results show that it is possible to add volume to the rear of the wing without increasing the drag of the forebody, thus confirming the proposed method of integration.

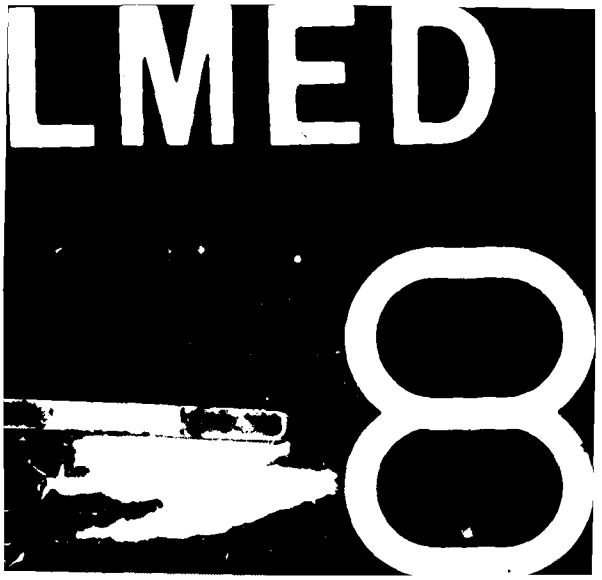
LMED
8